Accurate quantification of melt inclusion chemistry by LA-ICPMS

A comparison with EMP and SIMS and advantages and possible limitations of these methods

Accurate quantification of melt inclusion chemistry by LA-ICPMS: A comparison with EMP and SIMS and advantages and possible limitations of these methods

Thomas Pettke*, Werner E. Halter*, Jim D. Webster#, Mario Aigner-Torres*, and Christoph A. Heinrich*

* Isotope Geochemistry and Mineral Resources, Department of Earth Sciences, Federal Institute of Technology, ETH Zentrum NO, CH-8092 Zürich, Switzerland

Department of Earth and Planetary Sciences, A.M.N.H., Central Park West at 79th Street, New York, NY 10024-5192, USA

Corresponding author: Thomas Pettke
pettke@geo.unibe.ch

Please cite as:

Pettke, T., Halter, W. E., Webster, J. D., Aigner-Torres, M., and Heinrich, C. A., 2004. Accurate quantification of melt inclusion chemistry by LA-ICPMS: a comparison with EMP and SIMS and advantages and possible limitations of these methods. Lithos 78, 333-361.
DOI: 10.1016/j.lithos.2004.06.011

Abstract

Laser-ablation ICPMS has recently emerged as a powerful in-situ micro-analytical technique for major to trace elements in heterogeneous samples such as fluid and melt inclusions. Here, a rigorous comparison of melt inclusion (MI) data acquired by electron microprobe (EMP), ion microprobe (SIMS) and LA-ICPMS is used to evaluate the applicability and advantages/drawbacks of these approaches. We are specifically interested in determining if LA-ICPMS data on entire, unexposed, crystallized MI that cannot be homogenized in the lab are accurate and of a useful precision.

Quantification of LA-ICPMS MI signals requires the use of an internal standard, i.e., the concentration of one element, or an element ratio, at the time of MI entrapment must be known independently, in order to derive the pure MI composition from the MI plus host mixed signal. Analysis of plagioclase-hosted glassy MI of a MORB sample from the East Pacific Rise illustrates that melt inclusion chemistry can be accurately quantified by LA-ICPMS, including the correction for post-entrapment sidewall crystallization of the host mineral without prior reheating in the lab.

The LA-ICPMS data obtained on crystallized MI demonstrate agreement with the EMP and SIMS data on exposed glassy MI at the 1 standard deviation uncertainty level except for a few elements close to their limits of detection. LA-ICPMS data reduction schemes include the quantification of analytical uncertainty on each element of single MI. Therefore, weighted average element concentrations can be obtained for MI assemblages, at precisions that compare well with those of average element concentrations obtained by EMP and SIMS.

Simple sample preparation minimizing inclusion loss through polishing combined with the analytical efficiency of 50 inclusions plus neighbouring host mineral at up to 40 elements per day enable the collection of statistically relevant datasets by LA-ICPMS. These allow to recognize non-representative MI (e.g., heterogeneous entrapment). Application to individual clinopyroxene crystals from

the 79AD pumice horizon of Mt. Somma-Vesuvius reveals chemical variability that exceeds the analytical precision on single melt inclusions. This variability was not obvious from the limited dataset obtained by SIMS and EMP.

The largest source of non-quantifiable error for EMP and SIMS data stems from the requirement of reheating the melt inclusions in the lab in order to reverse post-entrapment crystallisation onto inclusion walls or growth of crystallites. For LA-ICPMS analysis of unexposed MI, the reliability with which the internal standard element concentration is known determines the quality of the data. LA-ICPMS, however, cannot analyse H_2O, F, S and Cl reliably, has higher LOD than SIMS for many elements for MI below ~25 μm, has lower spatial resolution than both EMP and SIMS and consumes much more sample per analysis. Therefore, EMP, SIMS and LA-ICPMS are complementary in MI research, and the type of application will determine the analytical method or methods of choice.

Keywords:
crystallized melt inclusions, analytical accuracy, inductively-coupled-plasma mass-spectrometry, secondary ion mass spectrometry

Introduction

Melt inclusions (MI) offer direct insight into the chemistry of the liquid phase present in a variety of igneous processes, including magma generation and crystallization, provided that no post-entrapment loss or gain of components has occurred. Moreover, MI can be trapped in various host minerals at successive stages of igneous evolution; hence MI can monitor the chemical evolution of the magmatic liquid with time. It is, thus, not surprising that the chemical analysis of MI is continuously drawing much attention (e.g., Roedder, 1979; Lowenstern, 1994; Danyushevsky et al., 2000, 2002a,b) and has provided unique constraints on igneous and magmatic-hydrothermal processes (e.g., Lu et al., 1992; Webster and Rebbert, 2001; Halter et al., 2002a, Audétat and Pettke, 2003).

The reliable chemical analysis of MI is a non-trivial task, however. The size of most MI commonly does not exceed a few tens of micrometers, so in-situ analysis by a microbeam technique is required. Electron microprobe (EMP) is routinely used to analyse major element compositions of MI. Secondary ion mass spectrometry (SIMS) has been employed in the past for trace elements, as it has been the only in-situ analytical technique with limits of detection in the sub-μg/g range for heavy trace elements (e.g., Shimizu and Hart, 1982), some of which are essential in petrogenetic modelling. SIMS also provides direct determination of H_2O, as H, and of halogens (most importantly Cl and F) in areas of silicate glass as small as ten μm (Ihinger et al., 1994). Both EMP and SIMS require a homogeneous sample, i.e., glassy MI, exposed to the sample surface. Therefore, a large group of crystallized MI that cannot be homogenized in the lab at entrapment temperatures due to loss of volatiles could so far not be reliably analysed for their major to trace element chemistry.

Laser-ablation inductively-coupled-plasma mass-spectrometry (LA-ICPMS) is a rapidly evolving in-situ micro-analytical technique, which allows the determination of most elements of the periodic table with limits of detection (LOD) that are comparable to those obtained by SIMS. Taylor et al. (1997)

demonstrated that the combination of a UV laser ablation microprobe (266 nm) with a quadrupole ICPMS provides both the spatial resolution and the sensitivity required for the successful in-situ analysis of individual silicate MI. Despite this huge potential, only limited attempts to analyse MI with LA-ICPMS are known from the literature, mainly for trace-element analysis of exposed glassy melt inclusions (e.g., Kamenetsky et al, 1998; Spandler et al., 2000; De Hoog et al., 2001). The analysis of entire, crystallized MI completely included in the host mineral has been limited to quartz and topaz (Audétat et al., 2000; Gunther et al., 2001), and quantification followed the same principles as those used for heterogeneous fluid inclusions (Heinrich et al., 2003). Other approaches used only the central signal section of homogeneous MI included in quartz or olivine for quantification (e.g., Taylor et al., 1997) or heterogeneous inclusions in clinopyroxene to obtain qualitative to semiquantitative results (Kamenetsky et al., 1999). Recent progress in the quantification of heterogeneous bulk MI entirely enclosed in chemically complex host minerals measured by LA-ICPMS (Halter et al., 2002b) now allows the analysis of MI that cannot be homogenized in the lab at entrapment temperatures. Such MI are often more abundant than those which can be homogenized, especially in association with shallow water-rich volcano-plutonic complexes. Another application of this technique is the chemical characterization of sulphide MI (Halter et al., 2002a) that hardly ever quench to a homogeneous glass, even at cooling rates exceeding 500 °C/s as available with some experimental equipment.

This paper presents a rigorous test of the accuracy of the mathematical deconvolution procedure of analytical data for MI included in chemically complex host minerals obtained by LA-ICPMS. It is our aim to show that heterogeneous unexposed MI that cannot be homogenized in the lab can be analysed accurately for their major- to trace-element contents and to define the uncertainties on such concentration data. Our accuracy test is based on a methods comparison between LA-ICPMS, SIMS and EMP, applied to three different types of MI, namely (i) natural glassy untreated, (ii) natural crystallized untreated and (iii) natural crystallized but reheated to a homogeneous glass. The petrologic

interpretation and significance of the MI data presented here are beyond the scope of this paper. Some of the MI data have been interpreted previously (Belkin et al., 1998; Raia et al., 2000; Webster et al., 2001, 2002), and interpretations of others will be published elsewhere.

Samples and analytical techniques

Two sample types that are representative of most of the MI analytical work to date were chosen for this investigation. We have analysed glassy MI hosted in plagioclase from a mid-ocean ridge basalt (MORB) collected by the submersible Alvin. We have also studied crystallized MI in clinopyroxene, both as untreated and reheated (i.e., homogenized to a glass), that are typical of volcanic rocks associated with volcano-plutonic centres at convergent margins. We make a strict distinction between MI populations and MI assemblages throughout this manuscript. MI assemblages define a series of individual MI trapped coevally along a petrographically defined growth zone of the host mineral. Provided that no boundary layer phenomena during entrapment and no post-entrapment modifications occurred, MI belonging to one assemblage are thus chemically identical samples entrapped at a specific stage of host phenocryst growth. MI populations on the other hand comprise all MI trapped in a specific host mineral of a sample, e.g., plagioclase or in clinopyroxene. One MI population may thus comprise a series of MI assemblages successively entrapped while the host phenocryst grew and the residual melt evolved, hence MI of a population can be chemically heterogeneous.

Sample ALV-3352-7, dredged from the southern East Pacific Rise, 17° – 19°S (STOWA cruise; Sinton et al., 1999), is a fresh MORB hand specimen with 1-3 mm phenocrysts of plagioclase (~10 vol.%, An_{82}), minor olivine (Fo_{86}) and traces of spinel in a glassy matrix. Plagioclase contains abundant glassy MI (10 – 300 μm) some of which show a shrinkage bubble (Fig. 1). Most of the MI occur in central parts of the plagioclase phenocrysts, while the outermost ~10 % of the crystal and a few hundred μm long plagioclase laths in the matrix are devoid of

MI. Since the chemical and geological data obtained from this spreading centre reveal nearly constant compositions with our sample representing a more primitive subset, it allows the study of liquid lines of descent applicable to the differentiation of tholeiitic magmas, where this plagioclase plays an important role. MI were not reheated prior to analysis.

Sample S19(2)b-201 is from the 79 AD pumice horizon of Mt. Somma-Vesuvius, Italy. Prior work on these tephriphonolitic, clinopyroxene-hosted MI has suggested that the concentrations of major and trace elements are remarkably reproducible from MI in a single sample (Raia et al., 2000; Webster et al., 2002). Our sample is generally representative of the chemically evolved pumice samples from this volatile-charged magmatic system of potassic-alkalic affinity. The rock consists predominantly of vesicular glass with less than 10 vol.% phenocrysts. Sanidine and clinopyroxene phenocrysts are most abundant with lesser biotite, leucite, and traces of Fe-Ti oxides. Sanidine phenocrysts range from 350 μm to less than 50 μm in length; clinopyroxene crystals are less than 250 μm in length, and biotites and leucites are typically less than 100 μm in diameter. Clinopyroxene hosts coarsely crystallized MI (up to 100 μm) the great majority of which are below 40 μm in diameter. For EMP and SIMS analysis, MI were homogenized by heating the clinopyroxene host phenocrysts at 1180-1200° C (1 atm) for two hours; the MI contain a shrinkage bubble with an estimated volume of 3 to 5 % on average after rehomogenization. Analysis of unexposed MI by LA-ICPMS was done on both reheated and crystalline MI, and two exposed MI analysed by EMP and SIMS were entirely ablated by LA-ICPMS.

LA-ICPMS: Table 1 provides a compilation of instrument and data acquisition parameters for LA-ICPMS MI analysis. The system at ETH Zürich consists of a pulsed 193 nm ArF Excimer laser (Lambda Physik, Germany) with an energy-homogenized (Microlas, Germany) beam profile (Günther et al., 1997) coupled with an ELAN6100 ICP quadrupole mass spectrometer (QMS; Perkin Elmer, Canada). The laser system is characterized by a laterally homogeneous energy distribution, allowing depth-controlled ablation of material at a rate of 0.1 to 0.2

μm per shot, depending on laser energy and matrix chemistry. The resulting ablation craters are flat-bottomed and slightly conical. The optical imaging system design permits the use of different pit diameters (8 - 100 μm) at constant energy density on the sample, by adjusting an aperture in the laser beam path. Simultaneous observation of the ablation process on the sample by a visual monitor and as real-time data signals is essential for controlled ablation of MI. The sample was loaded along with the SRM 610 glass standard from NIST in a 1 cm^3 ablation cell and put on the stage of a modified petrographic microscope. Laser-ablation aerosol was carried to the ICP-QMS by a mixed He-Ar carrier gas. A linear dynamic range of up to 8 orders of magnitude in dual detector mode (i.e., cross-calibrated pulse counting and analog detection), as provided by the ELAN6000 series QMS, is essential for the measurement of major (≤100 wt-%) to trace (≥ a few tens of ng/g^{-1}) elements, from a single analysis as required for MI.

Analyses were performed in sequence, and each ablation was stored individually as transient (i.e., time resolved) signal acquired in peak-hopping mode (Fig. 2). Two analyses on the external standard at the beginning and the end of each set, required for off-line data reduction, bracketed up to 16 analyses of unknowns. The certified glass standard SRM 610 was used as an external standard to calibrate analyte sensitivities, and bracketing standardization provided a linear drift correction. The analytical set-up was tuned for optimum performance across the entire mass range. Optimisation of the analytical set-up for a specific element can improve the limits of detection by up to an order of magnitude in the best case.

Data reduction of MI LA-ICPMS analyses is documented in great detail in Halter et al. (2002b), but we describe the approach briefly here. The general case of analysing entire MI enclosed in rock-forming silicate minerals (plus the rim of host mineral crystallized from the MI after entrapment), requires a means of deconvolving the LA-ICPMS signal into the contributions of pure host and pure MI. This is because the material sampled represents a mixture of host mineral and MI material (daughter mineral(s) with or without silicate glass) evolving in

unknown proportions during analysis. Halter et al. (2002b) have introduced four different approaches to do this and described the required equations and uncertainty calculations in great detail. Such MI plus host mixed analytical signals can be quantified provided that (a) all major and minor elements are recorded in the same LA-ICPMS signal to allow normalization of the mix signal to a fixed oxide total (Leach and Hieftje, 2000), and (b) the concentration of one element, or an element ratio, in the MI at the time of entrapment can be derived from independent constraints and used as an internal standard (IS).

Chronologically, a single shot analytical signal consists of a gas background, followed by a signal section of pure host, then the host+MI mixed signal, and finally the pure host signal again (Fig. 2). Background-corrected signal count rates are quantified by referring to a bracketing external standard (SRM 610) combined with internal standardization, respectively. Internal standardization of the analyses must be applied to correct for differences in sensitivity between SRM 610 and the samples, by defining the relative sensitivity factor, RSF. For MI quantification, this involves two steps. Firstly, the element concentrations of the mixed signal (Fig. 2) are quantified by normalizing to 100 wt-% element oxides (Leach and Hieftje, 2000) or less if components are present that could not be analysed, e.g., H_2O. Secondly, a fixed element concentration or an element ratio (the IS *sensu stricto*) is assigned to the pure MI in order to "unmix" the mixed signal into pure host and pure MI contributions. This step defines the mass ratio between the mass of the MI and the total mass of the mixed signal for each analysis individually. The significance of the internal standardization procedure will be addressed in detail below. Note that the pit diameter for laser drilling of the MI should be large enough so that ablation of the entire MI plus the rim crystallized after entrapment is ensured, but should be as small as possible in order to achieve the largest MI to host mass ratio (Halter et al., 2002b). If this ratio is smaller than about 0.1, the uncertainty on the pure MI composition becomes very large due to huge extrapolation to obtain the pure MI composition.

Limits of detection (LOD) for each signal interval were calculated for each element, for individual analyses, as three times the standard deviation of the gas

background signal divided by the element sensitivity (Longerich et al., 1996). For the calculation of the LOD for elements in the MI the reader is referred to the detailed discussion and formalism presented in Halter et al. (2002b). It is worth noting that smaller pit diameters result in higher LODs for a given element (for both the mineral and the MI, respectively), since the background signal remains the same while the analyte signal per concentration unit of the sample and unit time decreases approximately by the square of the radius of the pit diameter (for ideal ablation). This only applies in such a predictable way for laser systems (as that used here) that involve a homogeneous energy distribution across the entire sampled pit.

SIMS: The concentrations of H_2O, Li, Be, B, Rb, Sr, Y, Zr, Nb, Cs, Ce, Sm, Yb, Th, and U in the silicate glass of the MI were determined by SIMS (Cameca IMS-3f at the Woods Hole Oceanographic Institution) using modified methodologies of Shimizu and Hart (1982). For sample S19(2)b-201: the MI-bearing clinopyroxene phenocrysts were heated and rapidly quenched, mounted in epoxy, polished on one side, and coated with gold prior to analysis. The glasses of each inclusion were analysed 5 times each in one or two surface locations, and secondary ion counting times for each element ranged from 10 to 40 seconds. The samples were analysed at 12.5 keV and approximately 1 nA primary beam current using a focused ion beam of O^- that was typically ≥ 10 μm in diameter. However, as detailed below, these analytical conditions are not optimal for analyzing low concentrations of the heavy trace elements Cs, Th, U, and HREE. These conditions were not chosen to maximize the counting statistics and analytical precision for SIMS, but rather we chose a 1 na primary beam current and selected these specific counting times for each trace element in order to optimise the number of MI analysed (i.e., MI characterized by a geologically relevant range of sizes) while simultaneously acquiring analytical data with low but useful ranges of precision for most of the trace elements studied. Consequently, we report all acquired analytical SIMS data, but we note that precision of analyses for Rb, Cs, Th, U, and the HREE is poor because of the conditions used.

All constituents were analysed as high-energy ions to minimize the effects of mass interferences and reduce matrix effects, and only secondary ions with excess kinetic energies in the 78 ± 20 eV range were recorded. These analytical conditions have been carefully evaluated to confirm that potentially interfering masses of light and middle REE-oxides on the masses of measured HREE are minimized, following the extensive prior work of Shimizu and Hart (1982) on this potential problem. The secondary ion signal was accumulated with the instrument's electron multiplier, and electronic noise in the instrument can generate a very low number of false counts with an electron multiplier. Hence, the electron multiplier's background noise level was determined directly during each trace-element analysis by accumulating the number of counts for a non-existent low mass (i.e., a 'dummy' mass). All reported concentrations are background-subtracted values.

The counts for each positive ion of interest (X^+) were normalized to that of $^{30}Si^+$ for unknown and standard glasses, and working curves of concentrations versus ($X^+/^{30}Si^+$) were prepared for each element. The standard materials used include the SRM 610 and 612 glasses (H_2O, Li, Be, Rb, Sr, Y, Zr, Nb, Cs, Ce, Sm, Yb, Th, and U), the Macusani (Li, Rb, Y, Nb, Cs, and B) and Los Posos Rhyolite (H_2O) obsidians, and basaltic H_2O-bearing glasses prepared and analysed for H_2O by J. Dixon. The differences in the SiO_2 contents of each MI and the standard glasses were accounted for by normalizing the ($X^+/^{30}Si^+$) ratios to equivalent SiO_2 values. Analytical conditions for the trace elements of sample ALV-3352-7 were very similar except for the use of basaltic glass KL-2 as a standard (analyses also done at the Woods Hole Oceanographic Institution).

Based on counting statistics and these analytical conditions, the 1-sigma uncertainties (reported as % relative one standard deviation, RSD) for each element in the Mt. Somma-Vesuvius MI are as follows: 5 to 10 % RSD for Li, Be, B, Zr, Ce, and Sr; 15 to 25% RSD for Rb, Y, Nb and Sm; approximately 50% RSD for Cs; and 75 to 100% RSD for Yb, Th, and U. The reported water concentrations are reproducible to ± 0.3 wt.%.

The reproducibility values reported herein are a function of the total counts for each ion, which in turn vary with the maximum current of the primary ion beam and the counting times for the secondary ions. Low beam currents, like that used in this study, result in small primary beam sizes that permit analysis of small MI having diameters of 10 to 15 μm. However, such low beam currents also mean that the number of secondary ions collected for analysis is comparatively low and the limit of detection for some trace elements is correspondingly high. Conversely, higher primary beam currents consume a larger volume of glass, generate a larger secondary ion signal, and increase the limit of detection for trace-element analysis, but higher currents also involve larger primary beam sizes and preclude the analysis of relatively small MI. In other applications of SIMS, the analysis of larger MI may permit the use of comparatively larger primary currents, which involve more total counts for the secondary ions and improved counting statistics. Moreover, the counting statistics for secondary trace-element ions can be increased, and the LOD decreased, by increasing the counting times.

EMP: For sample S19(2)b-201: the concentrations of P_2O_5, SiO_2, SO_2, TiO_2, Al_2O_3, MgO, CaO, MnO, FeO, Na_2O, K_2O, F, and Cl in the silicate glass of the MI were determined with a Cameca SX-100 electron microprobe at the American Museum of Natural History using wavelength-dispersive techniques at 15 keV accelerating potential and 10 nA beam current for major and minor elements and 40 nA for S and Cl. These analyses were conducted with a defocused electron beam (4 μm diameter) and peak count times of 10 to 30 seconds. The samples were moved under the defocused beam during analysis to minimize Na, F, and K migration. The Cl concentrations were determined with 45 to 60 second count times, and replicate analyses on a single spot of glass show that the Cl counts are stable at these conditions. Sulphur K-alpha ˜wavelength scans were performed on these glasses to determine if the S peak conforms to that of anhydrite or troilite, and appropriate standard materials were used. Analytical uncertainties, based on 16 replicate analyses on different spots of a tephriphonolite glass, are: 1% RSD for CaO; 1.5% RSD for FeO, MgO, Cl, SiO_2

and Al_2O_3; 3% RSD for Na_2O and SO_2; 4% RSD for K_2O, F, and P_2O_5; and 25% RSD for TiO_2 and MnO.

For sample ALV-3352-7: major and minor elements were analysed with a Cameca SX-100 electron microprobe (Institute of Petrology, University of Vienna), which uses a 4-WDS with 1-EDS spectrometer combination. Analyses were done at 15 kV accelerating potential. For glass analysis the beam current was set to 10 nA (20 nA for minerals), defocused to 10 µm diameter - 1 µm for all other phases and for profiles to check for variations. Counting times for all phases were 20s on peak and 10s on background, except for Na and K in glass (10s/5s) and Fe, Mg, Ti and Mn in plagioclase - from 20 up to 50s on peak, in order to improve the counting statistics, resulting in 1-3% RSD. Calibrations were performed using different natural and synthetic phases as standards for both minerals and glasses. A natural augite crystal was measured as a running standard, with 1 standard deviations of 0.26 (SiO2), 0.03 (TiO_2), 0.04 (Al_2O_3), 0.06 (FeO), 0.02 (MnO), 0.07 (MgO), 0.09 (CaO), and 0.05 (Na_2O) wt.%, respectively.

Results and Discussion

The data obtained in this study by LA-ICPMS, SIMS and EMP are reported in various ways. Single MI analyses are reported for the LA-ICPMS data (appendix table 1 and 2), comprising each data point with its associated uncertainty calculated according to the data reduction scheme of Halter et al. (2002b). As no individual element uncertainties are available on single spot analyses by EMP and SIMS, these data are exclusively reported as simple average concentrations plus standard deviation uncertainties. In contrast, uncertainty-weighted averages plus associated uncertainties can be calculated for the LA-ICPMS data of MI assemblages. This is advantageous since precise analyses exert a larger influence on the resulting average than do imprecise data. Moreover, a mean square weighted deviates value (MSWD) can be obtained on the data used for averaging (Halter et al., 2002b), offering a means to check whether analytical uncertainties dominate the variability of the data (MSWD < ~3) or whether

chemical variability of the averaged population exceeds the analytical reproducibility of the data (MSWD > ~3). These statistical differences in reporting the data need appreciation in the following evaluation of the results.

The results on natural glassy, crystallized and reheated MI, their host plagioclase and clinopyroxene and the matrix glass of the MORB sample obtained by LA-ICPMS, SIMS and EMP are given in Tables 2 to 4 and are addressed in two groups. The glassy MI trapped in plagioclase of the MORB are discussed first, followed by the more complex case of crystallized MI variably enriched in volatile components (such as H_2O, SO_2, F and Cl) from Mt. Somma-Vesuvius (Webster et al., 2002). The data obtained by the various analytical techniques are compared in linear plots, rather than logarithmic plots, because the latter might obscure differences between datasets. A quantitative assessment of inherent uncertainties and accuracy of the data concludes this section. These examples are used here to illustrate the principles and reliability of the quantification procedure for unexposed, crystallized MI that cannot be homogenized in the lab.

Glassy MI of MORB sample ALV-3352-7

This sample was analysed for matrix glass, plagioclase and unheated glassy MI in it (Table 2). For the matrix glass, major-element analyses by EMP (~0.1 to 50 wt-%) and trace-element analyses by SIMS (~1 to 100 μg/g) agree well with the data obtained by LA-ICPMS (± 3% RSD on average, max. 17% for Nd). The LA-ICPMS results were obtained with a single 40-element menu (Table 2, Fig. 3a), which included additional trace elements such as Cs, Ta and Th in the one hundred ng/g range. Figure 3b shows that EMP and LA-ICPMS provide indistinguishable results for the host plagioclase, too, irrespective of whether Al_2O_3 or the summed element oxides are used as the internal standard. Note however, the lower analytical precision of LA-ICPMS major-element data compared to those obtained by EMP. The agreement between the three

analytical methods for silicate glass and crystals demonstrates that there is no inconsistency in the calibration strategies employed here.

EMP data of exposed MI (n=6) from different plagioclase crystals are uniform (Table 2), suggesting that the MI population trapped in plagioclase corresponds to an assemblage sensu stricto. This is plausible since only a few vol.% of plagioclase (see above) crystallized between earliest and latest possible entrapment of MI (i.e., any compositional differences among the MI are expected to be not resolvable even at the high analytical precision of EMP). Calibration of the LA-ICPMS data of unexposed MI by the use of MgO or FeO obtained from EMP on exposed MI as an IS results in values that agree well (except for TiO_2) with the EMP results of exposed MI (Fig. 3c), albeit at a lower analytical precision of the LA-ICPMS data. This proves that the numerical re-integration of MI compositions from mixed MI and host analytical signals using the equations presented in Halter et al. (2002b) is accurate.

It is well known from the literature that MI trapped in phenocrysts typically crystallise a rim of host mineral onto the inclusion walls after entrapment (e.g., Danyushevsky et al., 2002a). This is evidenced here by higher MgO and FeO and lower Al_2O_3 in the exposed MI compared to the matrix glass (Table 2), and by a small shrinkage bubble observed in some of the MI. The residual melt in the MI crystallized even more plagioclase than did the matrix glass. The following mathematical exercise shall illustrate different approaches to determining the composition of the MI at the time of entrapment from LA-ICPMS signals of whole unexposed MI that were not reheated prior to analysis. It is important to note that the results derived from these calculations are geologically reliable only for cases where there is no post-entrapment diffusive equilibration between MI and host phenocryst and when possible post-entrapment disequilibrium crystallisation of host mineral onto the inclusion walls is properly accounted for. These issues are a serious concern in MI research in general but beyond the scope of this paper, and the interested reader is referred to the literature (e.g., Lowenstern, 1995; Danyushevsky et al., 2000, 2002a,b).

The choice of the appropriate IS for quantification of LA-ICPMS data of unexposed MI can mathematically correct for post-entrapment crystallization of host mineral onto the MI walls, irrespective of equilibrium or disequilibrium crystallization, because during ablation of the entire MI the host mineral rim around the inclusion is analysed as well. The most reliable internal standard for this MORB sample is derived from petrologic model calculations, assuming that the MORB crystallized along the olivine – plagioclase cotectic. The intersection of the line of the reverse of olivine – plagioclase cotectic crystallization with that of the reverse of plagioclase crystallization onto MI walls after entrapment provides MgO = 8.48 wt.% at the time of MI entrapment (Fig. 4). Using the olivine – plagioclase – clinopyroxene cotectic crystallization results in a very similar MgO estimate. Plagioclase thus trapped, on average, MI of a composition that was slightly less evolved than that of the host glass, consistent with the petrographic evidence of small plagioclase laths in the matrix devoid of MI. The MI compositions derived from the LA-ICPMS data by using 8.48 wt.% MgO as the IS are reported in table 2. Figure 4 also illustrates that ~11wt.% plagioclase on average crystallized onto the MI walls after entrapment, demonstrating that the analysis of these exposed MI by EMP or SIMS without prior reheating results in precise but petrologically meaningless data.

The following calculations shall illustrate other approaches to defining an internal standard for quantification of the LA-ICPMS data and their relevance. It can be assumed that the melt trapped in inclusions is chemically identical to the matrix glass. This approach obviously corresponds to a minimal correction of post-entrapment sidewall crystallization because it assumes that crystallisation of the magma stopped immediately after the time of MI entrapment. In this case, any matrix glass element concentration can be used as an IS to calculate the chemical composition of the MI. If we now use the MgO composition of the matrix glass from EMP as an IS for the calculation of the chemical composition of the MI analysed by LA-ICPMS and compare these data with the EMP and LA-ICPMS analyses of the matrix glass, they are identical within uncertainty except for TiO_2, Y and Zr (Fig. 4b). Based on the EMP data of exposed MI this "minimal" fraction

of post-entrapment plagioclase crystallization onto the inclusion walls amounts to ~15 wt.% on average (Fig. 4, for calculation procedures refer to the figure caption). This is because plagioclase is admixed to the exposed MI concentration until its MgO corresponds to the MgO concentration of the matrix glass, not taking into account concurrent crystallization of olivine (recall that olivine is virtually absent as phenocryst in this hand specimen). A "maximum" correction of post-entrapment sidewall crystallization can be done using bulk rock element concentrations as an internal standard for the MI calculation (i.e., the MI was trapped at 0% crystallinity of the rock). Using the bulk rock MgO concentration of 7.86 wt.% as an IS for the calculation of the EMP data of exposed MI results in an admixture of 21 wt.% of plagioclase, on average, to the glassy MI. Although the trend of the resulting data is correct, the absolute values are incorrect (overcorrected for plagioclase crystallization), because the concurrent crystallization of olivine along the cotectic was neglected in these simple approaches. Figure 5 shows the above MI data normalized to the concentrations obtained by quantifying the MI data based on MgO = 8.48 wt.%. Deviations from the true value 1 exceed 10% and reveal an antithetic pattern for elements incompatible and compatible in the plagioclase host, respectively, unless the element concentrations are close to the respective limits of detection (e.g., Ta, Th and U in fig. 5, respectively).

Boundary layer effects at the time of MI entrapment cannot be resolved for the MORB, plagioclase-hosted MI (sample ALV-3352-7) that are larger than 15 μm, since element concentrations do not vary significantly as a function of the size of MI (15 - 35μm; Fig. 6). It has to be noted, however, that the analytical precision for single MI major-element data obtained by LA-ICPMS analysis of entire MI (especially those compatible in the host plagioclase) is quite low – precise EMP data would be needed to resolve this issue. Figure 5 also provides the uncertainty-weighted average element concentrations (± 2 standard deviations), demonstrating that precise data can be obtained from MI assemblages that were analysed as entire inclusions by LA-ICPMS.

Crystallized MI of samples from 79 AD pumice horizon, Mt. Somma-Vesuvius

Previously published results of 9 crystallized and reheated MI trapped in clinopyroxene phenocrysts from the 79AD pumice horizon of Mt. Somma-Vesuvius by EMP and SIMS (Webster et al., 2001) suggested a homogeneous MI population (the 1σ uncertainty of the results does not exceed 18% except for MnO, P_2O_5 and U, all of which with concentrations near their LOD). This is consistent with the observation that the MI homogenized at the same temperature conditions of 1180 – 1200° C (Belkin et al., 1998). The LA-ICPMS data obtained in this study, however, reveal a much wider range in MI compositions, and allow us to distinguish different MI assemblages hosted by chemically different clinopyroxene phenocrysts.

For this study, 12 different clinopyroxene grains of sample S19 were selected for analysis. Four grains containing crystallized MI were analysed by LA-ICPMS without prior homogenisation, and 8 grains were thermally homogenized for EMP and SIMS measurements. Seven MI of one of these reheated grains were then analysed by LA-ICPMS, 5 entirely included in the host clinopyroxene and two exposed MI previously measured by EMP and SIMS. For quantification of the LA-ICPMS signals of all MI, a volatile content of 5 wt.% (sum of H_2O, SO_2, F, Cl) and 14.8 wt.% Al_2O_3 as the IS have been employed (obtained from average values of the EMP data of 9 reheated MI; Table 3). Al_2O_3 is a suitable IS for the MI in this case because it is about three times enriched in the melt relative to the clinopyroxene and varies little with progressive melt fractionation or mixing (i.e., addition of portions of basic melt to the magma chamber prior to eruption). The mixed signals and the host clinopyroxene signals were quantified by normalizing to 100 wt.% element oxides.

The LA-ICPMS major- and trace-element data are reported together with the EMP/SIMS results in table 3. The LA-ICPMS results reveal two MI populations that are well resolved especially by the trace-element signatures (fig. 7a). These MI are hosted by chemically variable clinopyroxene phenocrysts (table 4). Comparison of the LA-ICPMS data of crystallized MI hosted by clinopyroxene

grain 2 and the reheated grain (used for SIMS analysis) reveals agreement for all elements within their associated 1 standard deviation uncertainties except for P_2O_5, Nd and Gd (fig. 7b). The fact that the MI of clinopyroxene grain 1 are different from the MI of grain 2 and the reheated grain could be interpreted to suggest that the host-mineral correction on the mix-signal for the MI of grain 1 may have been incorrect. By varying the factor of mass of MI divided by the total mass ablated (i.e., varying the proportions of pure MI and pure clinopyroxene host by changing the value of the IS; compare Halter et al., 2002b), no agreement of the MI chemistry between grain 1 and 2 or the reheated grain can be obtained, however. Chemically, the MI of grain 1 are less evolved than those of grain 2, the reheated grain, and 3 MI from grains 4 and 5, respectively. Comparison of the composition of the host clinopyroxene phenocrysts (Table 4) reveals that grain 1, grain 2 and the reheated grain are all chemically variable, notably in their trace-element patterns, despite the result that grain 2 and the reheated grain host chemically uniform MI (fig. 7b). The chemical variability between the clinopyroxene grains has been confirmed for the major elements by EMP (Table 4). It can be observed that the more primitive MI of grain 1 (indicated for example by lower Cs concentrations) are found in clinopyroxene phenocrysts characterized by a comparatively low Mg # (Table 4). Clearly, entrapment of MI in clinopyroxene occurred in a chemically evolving magma chamber. Averaging such MI data will hide compositional trends, and information on magma chamber processes such as magma mixing and fractional crystallization will inevitably be lost.

Comparison of the LA-ICPMS MI data with those obtained by EMP and SIMS is shown in figure 8, having rejected the LA-ICPMS data of the MI population hosted in clinopyroxene grain 1 as detailed above (20 MI; table 3). Agreement at the one standard deviation uncertainty level is demonstrated for all elements except Rb, Yb, Th and U, which are all lower in case of the SIMS data except for Yb that is more than double the LA-ICPMS value, probably due to oxide interferences. Yet the concentration of these elements as determined by LA-ICPMS is uniform for the MI hosted by three different clinopyroxene grains. The

Th/U ratio is notably sensitive to analytical bias in LA-ICPMS (e.g., Guillong and Günther, 2002), but the Th/U ratio is identical within uncertainty between the methods. This strongly suggests that the Th/U ratio measured by LA-ICPMS is correct. The discrepancies for Yb, Th, and U, between SIMS and LA-ICPMS are therefore ascribed to the low total counts recorded for these elements by SIMS and the low resulting 1-sigma precisions of 75 to 100 % relative for individual measurements (recall that the SIMS analytical conditions were optimised for the analysis of the more abundant trace elements). The discrepancy for Rb is 27 % relative which is also consistent with the 15 to 25% relative 1-sigma precision for individual SIMS measurements. Notable is the agreement for Li, Be and B (at the one standard deviation uncertainty level; Table 3), emphasizing that LA-ICPMS is well suited for the analysis of light elements. The agreement between the datasets obtained on crystallized and homogenized MI does also provide indirect evidence that homogenizing crystallized inclusions in the lab was successful for the Mt. Somma-Vesuvius samples. In conclusion, LA-ICPMS analysis of crystallized MI can provide accurate chemical compositions of bulk MI.

Statistics of the data of the three analytical methods

The reproducibility for large analyte signals (i.e., signals not limited by counting statistics) in LA-ICPMS is limited by sequential recording of a fluctuating signal. This arises from the overlay of low-frequency laser-ablation induced fluctuations (dependent on the aerosol transport system) on high-frequency plasma flicker and can, in the worst case, lead to non-representative sampling (Pettke et al., 2000). Typical one standard deviation uncertainties on the external reproducibility of wt.% to single μg/g element concentrations in multi-element mode are a few % RSD, and this analytical precision can be obtained on exposed glassy MI of >20 μm size. This is inferior to major-element EMP analyses but can compete well with trace-element SIMS data. As for SIMS, analyte signals near the LOD, which are roughly comparable between these methods for MI exceeding ~30 μm in diameter, will be dominated by the uncertainty resulting from counting statistics. And the LOD for a particular

element strongly depends on the analytical setup and machine tuning for both methods.

The data of the MI assemblage in MORB plagioclase are now used to illustrate the various analytical precisions for different data sets obtained by the three analytical techniques. For single MI drilled out of the host mineral by LA-ICPMS, the analytical uncertainty on their element composition is considerably larger than that estimated for EMP analysis of exposed glassy MI (Fig. 5, Table 2), largely due to the mathematical deconvolution of the mixed LA-ICPMS signal (Halter et al., 2002b). Consequently, average element concentrations from LA-ICPMS signals are also less precise than those obtained by EMP. Proper error-propagation of the LA-ICPMS single MI data (Halter et al., 2002b), however, provides the analytical uncertainty on each element concentration of a single MI. These data enable the calculation of error-weighted averages with uncertainties of only a few % at the 2 sigma level for MI assemblages. In contrast, EMP and SIMS element concentrations of single analytical spots do not have associated uncertainties, hence these data only allow the calculation of simple averages and standard deviation uncertainties. For example, the uncertainties on major element error-weighted averages of unexposed MI analysed by LA-ICPMS and on average EMP data for exposed MI are closely comparable, and the data overlap within the respective uncertainties except for Ti and Na (Table 2). Titanium in plagioclase-hosted MI is often problematic (e.g., Danyushevsky et al., 2002b), and the discrepancy of the Na values might be explained by loss of Na during the EMP analyses (note that the concentration of Na in the matrix glass is higher than that in plagioclase, Table 2). Moreover, calculation of the MSWD values for the weighted average LA-ICPMS MI data reveals that only K shows excessive scatter (MSWD value exceeding ~3), in support of our interpretation that the MI of the MORB sample represent an assemblage sensu stricto.

Uncertainty weighted averages provide the most accurate definition of the composition of a MI assemblage, at precisions that compare well with those obtained on average compositions calculated from EMP and SIMS data. This is because precise analyses exert a larger influence on the weighted average value

than do imprecise data. This has a large effect especially for elements with concentrations close to their LOD (recall that the LOD obtained by LA-ICPMS and by SIMS is lower for larger MI because a larger volume of sample is analysed per unit time) or for scattering results such as Sc or Cr of the reheated grain (Table 3). The MSWD values provide an independent check on whether or not natural chemical variability in the MI population exceeds analytical reproducibility. If so, a weighted average was calculated from multiple MI assemblages as illustrated in the case of the Mt. Somma-Vesuvius MI from the clinopyroxene grains 2, 4, 5 and "reheated" (table 3; MSWD up to 1460), potentially leading to erroneous interpretations. Illustrated in figure 6 is the fact that the precision on a weighted average element concentration commonly is of the order of only a few percent or less (unless close to the limit of detection), while the uncertainties associated with concentrations of single MI are much larger. LA-ICPMS of unexposed MI is therefore best suited to reliably and precisely constraining the average composition of MI assemblages.

Due to the statistically large number of analyses obtained by LA-ICPMS within one analytical session, it is easier to recognize and discard non-representative MI (Fig. 5, the Al_2O_3 value of a 20 μm MI or the K_2O value for a 25 μm MI). These include inclusions that have accidentally trapped a solid phase. Moreover, analyses of poor quality are also revealed, e.g., those stemming from non-representative sampling of tiny daughter crystals.

Tiny daughter crystals may contain a large proportion of some trace elements that produce a signal of one to two seconds only during laser ablation analysis. The highly transient nature of such signals may not be properly recorded in cases where the sequential measurement routine contains more than ~20 isotopes (elements). This is, however, the common case in bulk MI LA-ICPMS analysis. Therefore, even only partially homogenized MI should provide more reproducible analytical LA-ICPMS signals than do completely crystallized MI. Remelting redistributes the trace element content of such tiny daughter crystals across the MI, which results in longer, less variable signals, ensuring

representative sampling (compare Pettke et al., 2000). The data reported in table 3, however, do not allow to address this issue in more detail, since average data could only be obtained for populations that show chemical scatter exceeding the analytical uncertainty inherent in the single LA-ICPMS MI data (indicated by high MSWD, not shown). This most likely accounts for the observation that average element concentrations of the crystallized MI hosted by grain 2 are more precise than the average concentrations of the reheated MI. Single MI data of these two samples (table 2 appendix) do not provide conclusive evidence on this issue either. Our results illustrate rather the fact that other parameters such as the size of the MI and the quality of laser ablation exert the dominant influence on the overall analytical precision of LA-ICPMS analysis of unexposed MI, and these parameters obscure any possible trends in analytical precision between crystallized and reheated MI.

LA-ICPMS MI data for Zr of the Mt. Somma-Vesuvius sample have significantly larger uncertainties for grain 1 when compared to grain 2 (table 2 appendix). The clinopyroxene host crystals, however, have Zr concentrations that differ by a factor of 5 on average (Table 4). This illustrates that the uncertainty on the extrapolated MI composition increases with progressive compatibility of the element in the host mineral, which is plausible since the correction for host mineral addition to the mix signal becomes progressively more important. This comparison between average Zr concentrations and associated uncertainties demonstrates that elements relatively enriched in the host can also be quantified reliably, albeit to a lower precision. Therefore, if elements that are compatible in the host crystal are to be quantified in MI, measurements should be done whenever possible on exposed, reheated inclusions without ablation of the host phase.

Post-entrapment modification of MI compositions and the issue of internal standardization of LA-ICPMS signals

Two types of chemical post-entrapment modifications of MI need clear distinction, namely crystallization of host mineral onto the inclusion walls and diffusive re-equilibration with the host mineral at elevated temperatures. The former, but not the latter, is reversible through proper reheating of the MI (e.g., Danyushevsky et al., 2002a) as commonly applied in the past, or through modelling the reverse of host mineral crystallisation onto the inclusion walls (e.g., Danyushevsky et al., 2000; De Hoog et al., 2001). Our LA-ICPMS data for MI hosted in plagioclase demonstrate that internal standardisation for the quantification of MI is an accurate alternative, provided that some conditions are fulfilled by the IS element. The concentration of the IS element must correspond to that present at the time of MI capture by the host mineral and must not be affected by post-entrapment diffusive re-equilibration between MI and host mineral. For mafic host minerals, Fe and Mg are affected (Danyushevsky et al., 2002a; Halter et al., 2004), hence they should not be used as an internal standard element for MI quantification. Elements that are incompatible with the host are significantly less prone to re-equilibration than compatible ones (Danyushevsky et al., 2002b). There is a clear need, however, to better understand diffusional re-equilibration processes between MI host minerals and surrounding matrix melt as a function of entrapment temperature, host mineral and melt chemistries (notably the effect of the water content) and the cooling history of the samples.

Advantages and possible limitations of MI analysis by LA-ICPMS, EMP and SIMS

The parameter with the most non-quantifiable uncertainty, in homogenisation experiments of MI in the lab, is the amount of host mineral to be remelted into the inclusion in order to obtain the melt composition at the time of entrapment. LA-ICPMS analysis of unexposed MI does not require this sample preparation step,

because the entire MI plus any rim of host mineral crystallized onto the inclusion wall are accurately analysed during a single laser shot. However, the accurate quantification of the MI chemistry by LA-ICPMS relies on the availability of a correct internal standard, the determination of which is also a very delicate issue as illustrated here on the basis of the MORB sample. If one chooses the approach to characterize the melt evolution of a given system by using the chemical composition of successively entrapped MI assemblages, analytical precisions are comparable between LA-ICPMS, EMP and SIMS data sets. Therefore, the analyst has to choose between the uncertainties inherent in homogenizing MI in the lab and in deriving the IS element concentration, except for MI that cannot be homogenized in the lab. LA-ICPMS analysis of unexposed MI should also be considered as a check on the quality of the data obtained by EMP and SIMS on remelted MI.

LA-ICPMS is a cost and time efficient analytical method. Fifty MI plus host mineral pairs can be analysed in one analytical day for a very large number of major to trace elements down to sub-μg/g concentrations (depending on MI size). It was demonstrated that the extensive LA-ICPMS dataset of MI and host clinopyroxene measured in one analytical day allows resolution of sample heterogeneities that were not apparent from the limited trace-element data set obtained by SIMS, because SIMS cannot match this analytical efficiency. While EMP can match it from the point of view of analysis time, it is limited by the number of exposed MI available per sample for analysis and to element concentrations exceeding ~50 to 100 μg/g.

Each host mineral is measured adjacent to the MI under identical analytical conditions (i.e., within one recorded shot), allowing direct determination of apparent partition coefficients for major to trace elements. Loss through polishing is also minimized in case of LA-ICPMS analysis of unexposed MI. This is particularly important for a statistically significant characterization of MI assemblages, e.g., MI trapped in a primary growth zone of a phenocryst. The

obvious drawback of LA-ICPMS is that the entire MI is consumed during analysis rendering a revisit impossible.

Matrix-matching standardization at similar concentration levels (mandatory for SIMS and recommended for EMP) is not required for the LA-ICPMS set-up employed here. Therefore, extremely well characterized and widely used certified glass standards such as the NBS series from the US-NIST can be used for the quantification of silicate (and sulphide; Halter et al., 2002a) MI trapped in silicate or oxide minerals (see also Heinrich et al., 2003). This improves the comparability of data generated in different labs and thus ultimately the reliability of results.

SIMS and EMP also have distinct advantages over LA-ICPMS. Species such as H_2O (measured as H), F, S and Cl are currently not accessible in silicates by LA-ICPMS, because the first positive ionisation potential of F is too high; of molecular O interferences on S unless a high-resolution magnetic sector ICPMS is employed; and of very poor ionisation efficiency for Cl resulting in LODs of the order of 1 wt.% or even higher. These elements are reliably measured by SIMS or EMP. SIMS has higher spatial resolution with detection capabilities similar to LA-ICPMS. MI < 10 μm analysed for trace elements with LA-ICPMS have LOD of the order of a few tens to 100 μg/g, which are inferior to those obtained by SIMS for such samples, namely for the novel technique of nano-SIMS (e.g., Stadermann, 2002). SIMS and EMP consume much lower sample amounts per unit time, hence they may be the only choice for cases where only limited quantities of sample are available. Finally, external standardization alone can be reliable for EMP analysis of exposed MI, while LA-ICPMS and SIMS require independent knowledge of a reliable IS to be used for deconvolution of the mixed host + MI signal into pure MI, which can be a non-trivial issue as illustrated above. One way of quantifying LA-ICPMS data (Halter et al., 2002b) is by determination of an IS through the analysis of homogeneous MI by EMP or possibly SIMS. These considerations illustrate that more than one analytical technique is required for the complete chemical characterization of MI. The

analytical techniques complement each other, hence the best choices are dictated by the geological application.

Conclusions

The chemical analysis of MI requires in-situ micro-analytical techniques of which the EMP and SIMS have widely been used. The most recent progress in LA-ICPMS analysis has prompted an evaluation of its accuracy for the analysis of heterogeneous (i.e., crystallized) bulk MI from beneath the sample surface. Such inclusions could so far not be analysed reliably except for cases where they could be reheated to a homogeneous glass.

Bulk MI are accurately analysed for major- to trace-element concentrations with LA-ICPMS, be they crystallized or glassy and be they exposed or beneath the sample surface. The precisions on average element concentrations of MI assemblages sensu stricto are comparable between the three analytical methods when error-weighted averages as obtained by LA-ICPMS (Halter et al., 2002b) are compared to averages as obtained by EMP or SIMS (the latter two techniques lacking a commonly accepted way of determining the analytical uncertainty on single data points). Counting statistics provide an approximate estimate of the uncertainty associated with a single analysis, particularly near the LOD, but other variables also contribute to this uncertainty. The analysis of entire MI drilled out of the sample by LA-ICPMS thus enables the accurate quantification of MI chemistry for samples that cannot be homogenized in the lab, e.g., because of loss of volatile species such as H during the geological history of the sample or the homogenisation experiment or because of instantaneous nuggetting as observed e.g., for Au in sulphide melts. It is foreseen that analyses of heterogeneous MI may become the main field of LA-ICPMS MI analysis.

The requirement of an independently known internal standard for the quantification of MI measurements by LA-ICPMS may be considered the single most important limitation of this approach – or it may be understood as the key to obtaining accurate results from possibly heterogeneous MI analysed in bulk. The

choice of an internal standard element is delicate and currently suffers most from the limited knowledge of the existence and extent of post-entrapment diffusional re-equilibration of potential IS elements between the MI and host mineral – processes that need a better understanding for MI research in general. Currently, the analyst has to choose between the ambiguities inherent in the thermal homogenisation procedures (e.g., Danyushevsky et al., 2002a) required for EMP and SIMS MI analysis and the uncertainties associated with internal standardization required for the quantification of LA-ICPMS data.

LA-ICPMS is inferior to EMP and SIMS concerning the spatial resolution, the LOD for some trace elements in MI < 10 µm in diameter and, to date, cannot analyse H_2O, F, S and Cl reliably. New-generation ICPMS instruments may overcome some of these limitations, e.g.,the use of high-resolution sector field instruments (Latkoczy and Günther, 2002; Evans et al., 2001) or the dynamic reaction cell technology (e.g., Hattendorf and Günther, 2000) to minimize problems of interferences. Moreover, external standardization alone can be reliable for EMP analysis of exposed MI. On the other hand, the minimized loss of MI through polishing (no exposure of MI required for analysis), the large sample throughput (~50 MI plus host minerals at ≤40 major to trace elements per day possible) and the matrix and concentration insensitive external calibration of the LA-ICPMS setup used here are notable advantages for the analysis of MI by LA-ICPMS. LA-ICPMS, EMP and SIMS are therefore considered as complementary techniques, whereby the application determines which methods are most suitable.

We predict that the analysis of heterogeneous (i.e., crystallized) MI will become a main domain of future LA-ICPMS MI applications, and that this approach can be expanded to the analysis of heterogeneous mineral inclusions, e.g., those that suffer from post-entrapment exsolution of one phase from another. It will cover most MI studies dealing with hydrous volcano-plutonic centres and volatile-rich plutonic magmas genetically associated with mineralisation. The reliable characterization of sulphide MI may only now have

become possible, because sulphide melts rarely quench to a homogeneous glass.

Acknowledgments

We acknowledge N. Shimizu and G. Layne for helping with the SIMS measurements (sample ALV-3352-7) at WHOI, T. Ntaflos from the Univ. of Vienna for support with the EMPA analysis (sample ALV-3352-7), and the assistance of Christine Tappen in the electron microprobe analyses of Mt. Somma-Vesuvius melt inclusions and host grains (sample S19). MAT kindly thanks J. Sinton for providing the samples from the R/V Atlantis cruise 3-31. The very insightful reviews of L. Danyushevsky, R.L. Hervig, and M. Tiepolo, and the comments by editor-in-chief S. Foley helped to considerably improve the focus of the manuscript. Partial support for this study was provided by the Swiss National Science Foundation to CAH.

References

Audetat, A., Pettke, T., 2003. The magmatic-hydrothermal evolution of two barren granites: a melt and fluid inclusion study of the Rito del Medio and Canada Pinabete plutons in northern New Mexico (USA). Geochimica et Cosmochimica Acta 67(1), 97-121.

Audetat, A., Günther, D., Heinrich, C.A., 2000. Magmatic-hydrothermal evolution in a fractionating granite: a microchemical study of the Sn-W-F-mineralized Mole Granite (Australia). Geochimica et Cosmochimica Acta 64(19), 3373-3393.

Belkin, H.E., De Vivo, B., Torok, K., Webster, J.D., 1998. Pre-eruptive volatile content, melt-inclusion chemistry, and microthermometry of interplinian Vesuvius lavas (pre-AD1631). Journal of Volcanology and Geothermal Research 82(1-4), 79-95.

Danyushevsky, L.V., 2001. The effect of small amounts of H_2O on crystallisation of mid-ocean ridge and backarc basin magmas. Journal of Volcanology and Geothermal Research 110(3-4), 265-280.

Danyushevsky, L.V., Della-Pasqua, F.N., Sokolov, S., 2000. Re-equilibration of melt inclusions trapped by magnesian olivine phenocrysts from subduction-related magmas: petrological implications. Contributions to Mineralogy and Petrology 138(1), 68-83.

Danyushevsky, L.V., McNeill, A.W., Sobolev, A.V., 2002a. Experimental and petrological studies of melt inclusions in phenocrysts from mantle-derived magmas: an overview of techniques, advantages and complications. Chemical Geology 183(1-4), 5-24.

Danyushevsky, L.V., Sokolov, S., Falloon, T.J., 2002b. Melt inclusions in olivine phenocrysts: Using diffusive re- equilibration to determine the cooling history of a crystal, with implications for the origin of olivine-phyric volcanic rocks. Journal of Petrology 43(9), 1651-1671.

de Hoog, J.C.M., Mason, P.R.D., van Bergen, M.J., 2001. Sulfur and chalcophile elements in subduction zones: Constraints from a laser ablation ICP-MS study of melt inclusions from Galunggung Volcano, Indonesia. Geochimica et Cosmochimica Acta 65(18), 3147-3164.

Evans, P., Wolff-Briche, C., Fairman, B., 2001. High accuracy analysis of low level sulfur in diesel fuel by isotope dilution high resolution ICP-MS, using silicon for mass bias correction of natural isotope ratios. Journal of Analytical Atomic Spectrometry 16(9), 964-969.

Guillong, M., Günther, D., 2002. Effect of particle size distribution on ICP-induced elemental fractionation in laser ablation-inductively coupled plasma-mass spectrometry. Journal of Analytical Atomic Spectrometry 17(8), 831-837.

Günther, D., Frischknecht, R., Heinrich, C.A., Kahlert, H.J., 1997. Capabilities of an argon fluoride 193 nm excimer laser for laser ablation inductively coupled plasma mass spectrometry microanalysis of geological materials. Journal of Analytical Atomic Spectrometry 12(9), 939-944.

Günther, D., Hattendorf, B., Audétat, A., 2001. Multi-element analysis of melt and fluid inclusions with improved detection capabilities for Ca and Fe using laser ablation with a dynamic reaction cell ICP-MS. Journal of Analytical Atomic Spectrometry 16(9), 1085-1090.

Halter, W.E., Pettke, T., Heinrich, C.A., 2002a. The origin of Cu/Au ratios in porphyry-type ore deposits. Science 296(5574), 1844-1846.

Halter, W.E., Pettke, T., Heinrich, C.A., Rothen-Rutishauser, B., 2002b. Major to trace element analysis of melt inclusions by laser-ablation ICP-MS: methods of quantification. Chemical Geology 183(1-4), 63-86.

Halter W.E., Pettke T., Heinrich C.A. (2004) Laser-ablation ICP-MS analysis of melt inclusions in an andesitic complex I: Analytical approach and data evaluation. Contributions to Mineralogy and Petrology, accepted pending revisions.

Hattendorf, B., Günther, D., 2000. Characteristics and capabilities of an ICP-MS with a dynamic reaction cell for dry aerosols and laser ablation. Journal of Analytical Atomic Spectrometry 15(9), 1125-1131.

Heinrich, C.A., Pettke, T., Halter, W.E., Aigner-Torres, M., Audétat, A., Günther, D., Hattendorf, B., Bleiner, D., Guillong, M., Horn, I., 2003. Quantitative multi-element analysis of minerals, fluid and melt inclusions by laser-ablation inductively-coupled-plasma mass- spectrometry. Geochimica Et Cosmochimica Acta 67(18), 3473-3497.

Ihinger, R., Hervig, R., McMillan, P., 1994. In: Carroll, M.R., Holloway, J.R. (Eds.), Analytical methods for volatiles in glasses, *in* Volatiles in Magmas, MSA Reviews in Mineralogy 30, pp. 67-121.

Kamenetsky V. S., Eggins S. M., Crawford A. J., Green D. H., Gasparon M., Falloon T. J., 1998. Calcic melt inclusions in primitive olivine at 43 degrees N MAR: evidence for melt-rock reaction/melting involving clinopyroxene-rich lithologies during MORB generation. Earth and Planetary Science Letters 160(1-2), 115-132.

Kamenetsky, V.S., Wolfe, R.C., Eggins, S.M., Mernagh, T.P., Bastrakov, E., 1999. Volatile exsolution at the Dinkidi Cu-Au porphyry deposit, Philippines: A melt-inclusion record of the initial ore-forming process. Geology 27(8), 691-694.

Latkoczy, C., Günther, D., 2002. Enhanced sensitivity in inductively coupled plasma sector field mass spectrometry for direct solid analysis using laser ablation (LA-ICP-SFMS). Journal of Analytical Atomic Spectrometry 17(10), 1264-1270.

Leach, A.M., Hieftje, G.M., 2000. Methods for shot-to-shot normalization in laser ablation with an inductively coupled plasma time-of-flight mass spectrometer. Journal of Analytical Atomic Spectrometry 15(9), 1121-1124.

Longerich, H.P., Jackson, S.E., Günther, D., 1996. Laser ablation inductively coupled plasma mass spectrometric transient signal data acquisition and

analyte concentration calculation. Journal of Analytical Atomic Spectrometry 11(9), 899-904.

Lowenstern, J.B., 1994. Dissolved volatile concentrations in an ore-forming magma. Geology 22(10), 893-896.

Lowenstern, J.B., 1995. Applications of silicate-melt inclusions to the study of magmatic volatiles. In: F.H. Thompson (Ed.), MAC Short Course Series 23, pp. 71-99.

Lu, F.Q., Anderson, A.T., Davis, A.M., 1992. Melt inclusions and crystal-liquid separation in rhyolitic magma of the Bishop Tuff. Contributions to Mineralogy and Petrology 110(1), 113-120.

Pettke, T., Heinrich, C.A., Ciocan, A.C., Günther, D., 2000. Quadrupole mass spectrometry and optical emission spectroscopy: detection capabilities and representative sampling of short transient signals from laser-ablation. Journal of Analytical Atomic Spectrometry 15(9), 1149-1155.

Raia, F., Webster, J.D., De Vivo, B., 2000. Pre-eruptive volatile contents of Vesuvius magmas: constraints on eruptive history and behavior. I - the medieval and modern interplinian activities. European Journal of Mineralogy 12(1), 179-193.

Roedder, E., 1979. Origin and significance of magmatic inclusions. Bulletin de Minéralogie 102(5-6), 487-510.

Shimizu, N., Hart, S.R., 1982. Applications of the ion microprobe to geochemistry and cosmochemistry. Annual Review of Earth and Planetary Sciences, 10, 483-526.

Sinton, J., Bergmanis, E, Batiza, R., Rubin, K., Gregg, T., Grönvold, K., White, S., Macdonald, K., Van Dover, C., Cormier, M., Ryan, W., Aigner-Torres, M., Popels, L., Boyle, E., Shah, A. and Jin, W. (1999) Volcanological investigations at superfast spreading: results from R/V Atlantis cruise 3-31. Ridge Events 10, 17–23.

Spandler, C.J., Eggins, S.M., Arculus, R.J., Mavrogenes, J.A., 2000. Using melt inclusions to determine parent-magma compositions of layered intrusions: application to the Greenhills Complex (New Zealand), a platinum group minerals-bearing, island-arc intrusion. Geology 28(11), 991-994.

Stadermann, F.J., 2002. Isotopic and elemental studies at a 50 nm scale with the NanoSIMS (abstract). Geochimica et Cosmochimica Acta 66(15A), A734-A734.

Taylor, R.P., Jackson, S.E., Longerich, H.P., Webster, J.D., 1997. In situ trace-element analysis of individual silicate melt inclusions by laser ablation microprobe inductively coupled plasma-mass spectrometry (LAM-ICP-MS). Geochimica et Cosmochimica Acta 61(13), 2559-2567.

Webster, J.D., Rebbert, C.R., 2001. The geochemical signature of fluid-saturated magma determined from silicate melt inclusions in Ascension Island granite xenoliths. Geochimica et Cosmochimica Acta 65, 123-136.

Webster, J.D., De Vivo, B., 2002. Experimental and modeled solubilities of chlorine in aluminosilicate melts, consequences of magma evolution, and implications for exsolution of hydrous chloride melt at Mt. Somma-Vesuvius. American Mineralogist 87(8-9), 1046-1061.

Webster, J.D., Raia, F., De Vivo, B., Rolandi, G., 2001. The behavior of chlorine and sulfur during differentiation of the Mt. Somma-Vesuvius magmatic system. Mineralogy and Petrology 73(1-3), 177-200.

Figure Captions

Fig. 1. Samples used in this study. (a) Polished thick section of MORB ALV-3352-7 showing plagioclase phenocrysts with glassy melt inclusions some of which show a shrinkage bubble. (b) Embedded clinopyroxene grain of Mt. Somma-Vesuvius sample S19(2)b-201 (grain 2) showing numerous crystallized melt (black spots) and mineral inclusions.

Fig. 2. Transient LA-ICPMS signal of selected elements produced from ablation of a 30μm crystallized melt inclusion in clinopyroxene of Mt. Somma-Vesuvius sample S19(2)b-201. Signal intervals "Background", "Mixed signal" and "Host" define the respective integration intervals used for quantification as described in text. Note that some of the signals (e.g., Fe, Ba, P) clearly show heterogeneous element distribution within the melt inclusion.

Fig. 3. Plots comparing data obtained by LA-ICPMS, EMP and SIMS for sample MORB ALV-3352-7. (a) Matrix glass, (b) plagioclase phenocrysts, and (c) glassy melt inclusions in plagioclase. Filled circles show major elements in wt. % oxides, filled triangles show trace elements in μg/g. Empty symbols denote element concentrations that do not agree between the analytical methods within the 1 standard deviation uncertainty (compare Table 2) shown as error bars. IS describes the type of internal standard used for the quantification of the LA-ICPMS signals.

Fig. 4. Diagram of Al_2O_3 vs MgO used to define the petrologically most reliable internal standard for quantification of LA-ICPMS melt inclusion data of unexposed melt inclusion of the MORB sample ALV-3352-7. Modelling of the reverse trend of olivine – plagioclase cotectic crystallization was done using Petrolog (Danyushevsky, 2001), and the filled circles show 0.5 wt.% crystallization increments. Modeling of the reverse trend of plagioclase crystallization onto MI walls was based on measured partition coefficients between plagioclase and host glass and the average composition of MI as determined by EMP (table 2), and the filled squares show 0.5 wt.%

crystallization increments. The intersection of these lines thus corresponds to the average composition of the MI assemblage at the time of entrapment. This plot also shows that ~11 wt.% of plagioclase, on average, crystallized onto the inclusion walls after entrapment.

Fig. 5. Diagram showing the LA-ICPMS results of unexposed melt inclusion (MORB sample ALV-3352-7) calculated by using different MgO concentrations (as explained in text), normalized to the values obtained by using 8.48 wt.% MgO (obtained from modelling the reverse of olivine – plagioclase cotectic crystallisation as illustrated in figure 4). Deviation from the true element concentrations (normalized value = 1) exceed 10% in some cases and generally show an antithetic pattern for elements incompatible and compatible in the plagioclase host, respectively.

Fig. 6. Selected major- to trace-element concentrations of plagioclase-hosted, unexposed single MI (MORB sample ALV-3352-7) analysed by LA-ICPMS plotted against the size of melt inclusion . Element oxides are in wt.%, trace elements in μg/g, and associated uncertainties are 2 standard deviations. Note that outliers can readily be identified (e.g., Al_2O_3 for a 20 μm melt inclusion) and thus be discarded. The dashed black line shows the uncertainty-weighted averages with its associated one standard deviation uncertainty, demonstrating that precise assemblage data on unexposed melt inclusion can be obtained by LA-ICPMS (see text for further discussion of statistical figures).

Fig. 7. Comparison of average LA-ICPMS data of crystallized melt inclusion populations analysed as unexposed inclusions in three different clinopyroxene grains from Mt. Somma-Vesuvius. The melt inclusion population of grain 1 differs from that of grain 2 (a) and the reheated grain (not shown), while the latter two are chemically uniform with P_2O_5 as a notable outlier (c). Filled circles show major elements in wt.% oxides, filled triangles show trace elements in μg/g. Empty symbols denote element concentrations that do not agree between the analytical methods within the 1 standard deviation

uncertainty (compare Table 3) shown as error bars. IS defines the IS element concentration used for the LA-ICPMS signal quantification.

Fig. 8. Comparison of the average element concentrations of the population of melt inclusion quantified by EMP and SIMS with that analysed by LA-ICPMS (table 3), not including those melt inclusion hosted by grain 1 (as detailed in text). All average concentrations agree within their plotted 1 standard deviation uncertainties (error bars) except those for U, Th, Yb and Rb (empty symbols). The discrepancy for these elements is ascribed partly to the variability of melt inclusion compositions within the averaged population (as evidenced by large MSWD values; table 3) and partly to the non-optimum SIMS analytical conditions for these elements.

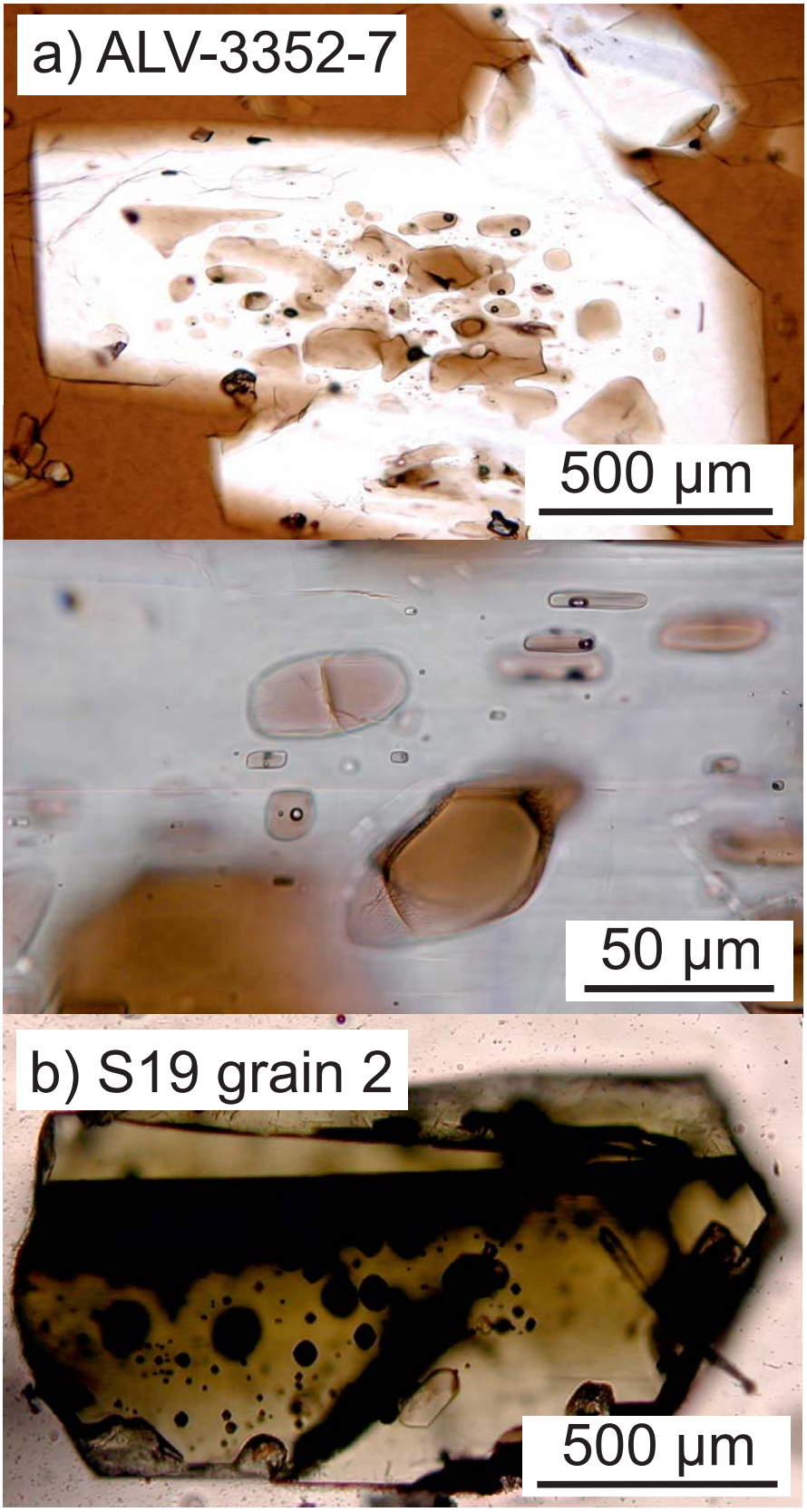
a) ALV-3352-7
500 µm
50 µm
b) S19 grain 2
500 µm

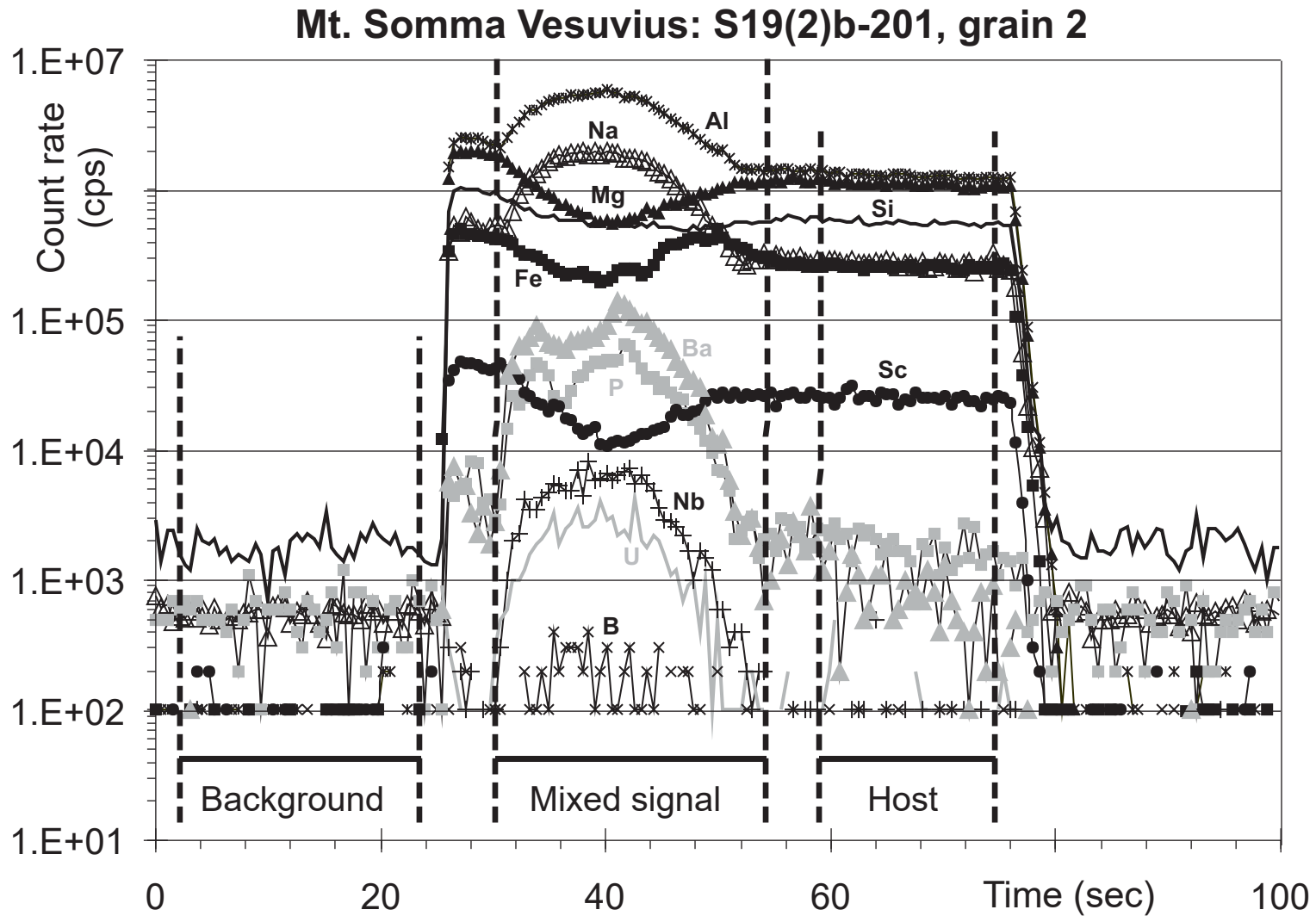
Mt. Somma Vesuvius: S19(2)b-201, grain 2
Count rate (cps)
1.E+07
1.E+05
1.E+04
1.E+03
1.E+02
1.E+01
Al
Na
Mg
Si
Fe
Ba
P
Sc
Nb
U
B
Background
Mixed signal
Host
0
20
40
60
Time (sec)
100

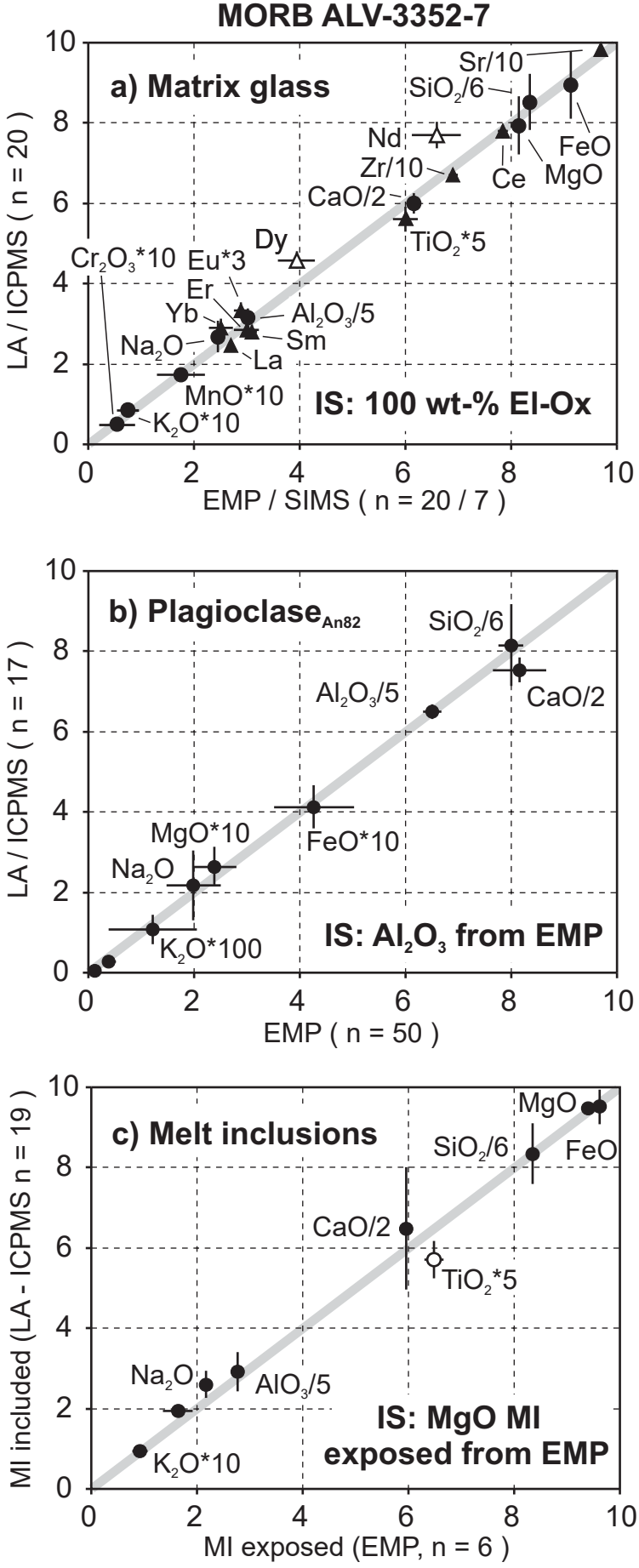
MORB ALV-3352-7
a) Matrix glass
IS: 100 wt-% EI-Ox
LA / ICPMS (n = 20)
EMP / SIMS (n = 20 / 7)
Sr/10
SiO2/6
Nd
Zr/10
CaO/2
TiO2*5
Dy
Cr2O3*10
Eu*3
Er
Yb
Al2O3/5
Na2O
Sm
La
MnO*10
K2O*10
FeO
MgO
Ce
b) Plagioclase An82
IS: Al2O3 from EMP
LA / ICPMS (n = 17)
EMP (n = 50)
SiO2/6
Al2O3/5
CaO/2
FeO*10
MgO*10
Na2O
K2O*100
c) Melt inclusions
IS: MgO MI exposed from EMP
MI included (LA - ICPMS n = 19)
MI exposed (EMP, n = 6)
MgO
SiO2/6
FeO
CaO/2
TiO2*5
Na2O
AlO3/5
K2O*10

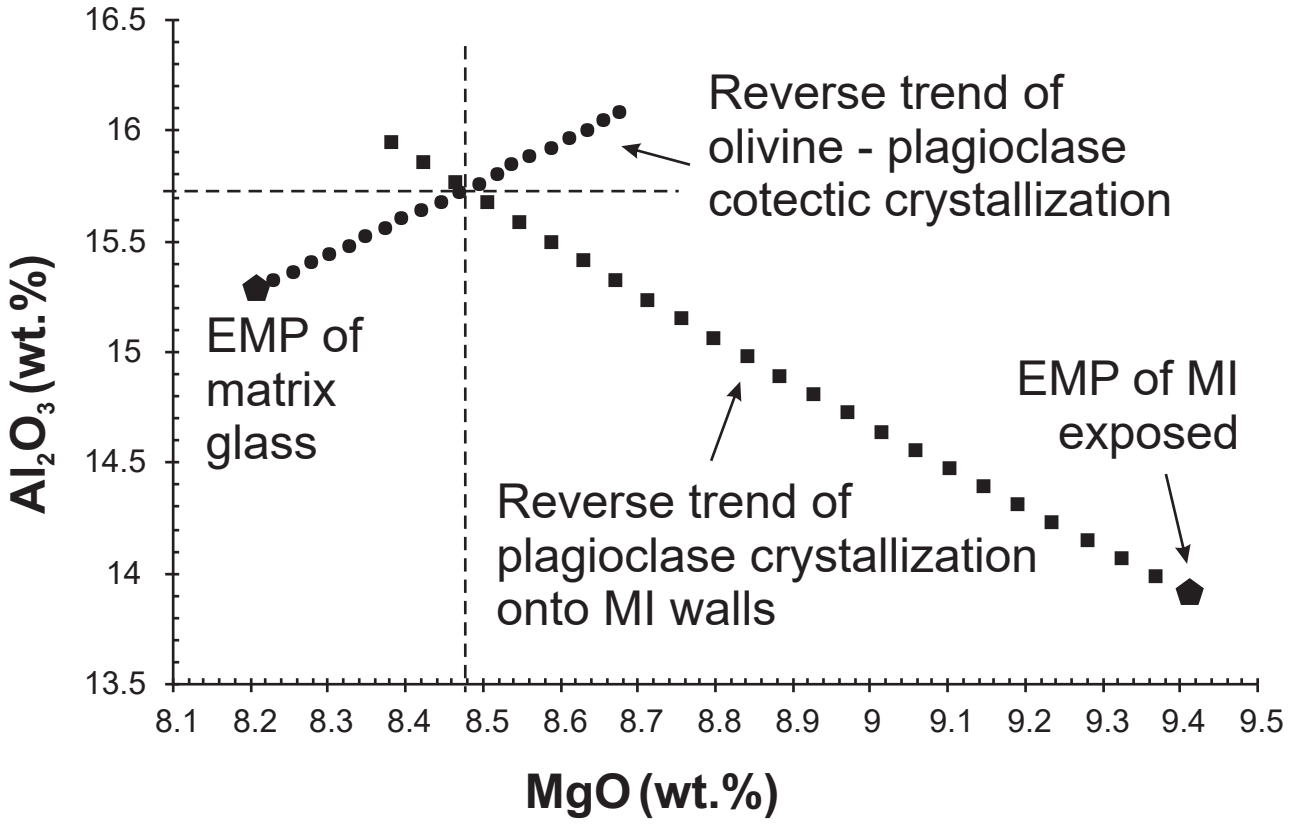
16.5
16
15.5
15
14.5
14
13.5
8.1
8.2
8.3
8.4
8.5
8.6
8.7
8.8
8.9
9
9.1
9.2
9.3
9.4
9.5
Al2O3 (wt.%)
MgO (wt.%)
Reverse trend of
olivine - plagioclase
cotectic crystallization
EMP of
matrix
glass
EMP of MI
exposed
Reverse trend of
plagioclase crystallization
onto MI walls

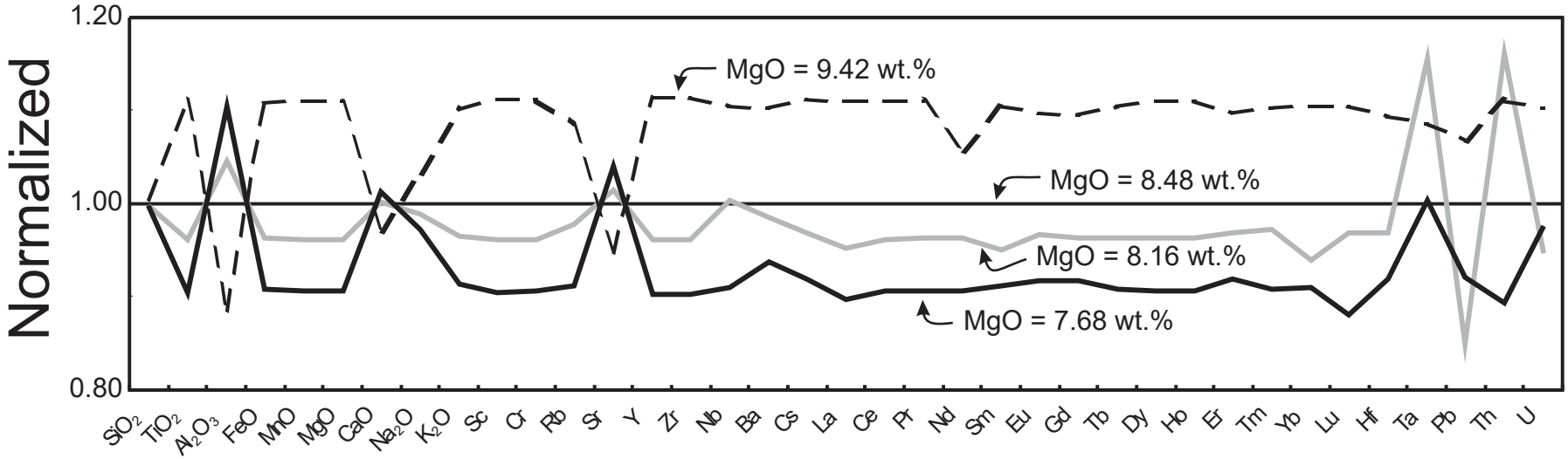
Normalized
1.20
1.00
0.80
MgO = 9.42 wt.%
MgO = 8.48 wt.%
MgO = 8.16 wt.%
MgO = 7.68 wt.%
SiO2
TiO2
Al2O3
FeO
MnO
MgO
CaO
Na2O
K2O
Sc
Cr
Rb
Sr
Y
Zr
Nb
Ba
Cs
La
Ce
Pr
Nd
Sm
Eu
Gd
Tb
Dy
Ho
Er
Tm
Yb
Lu
Hf
Ta
Pb
Th
U

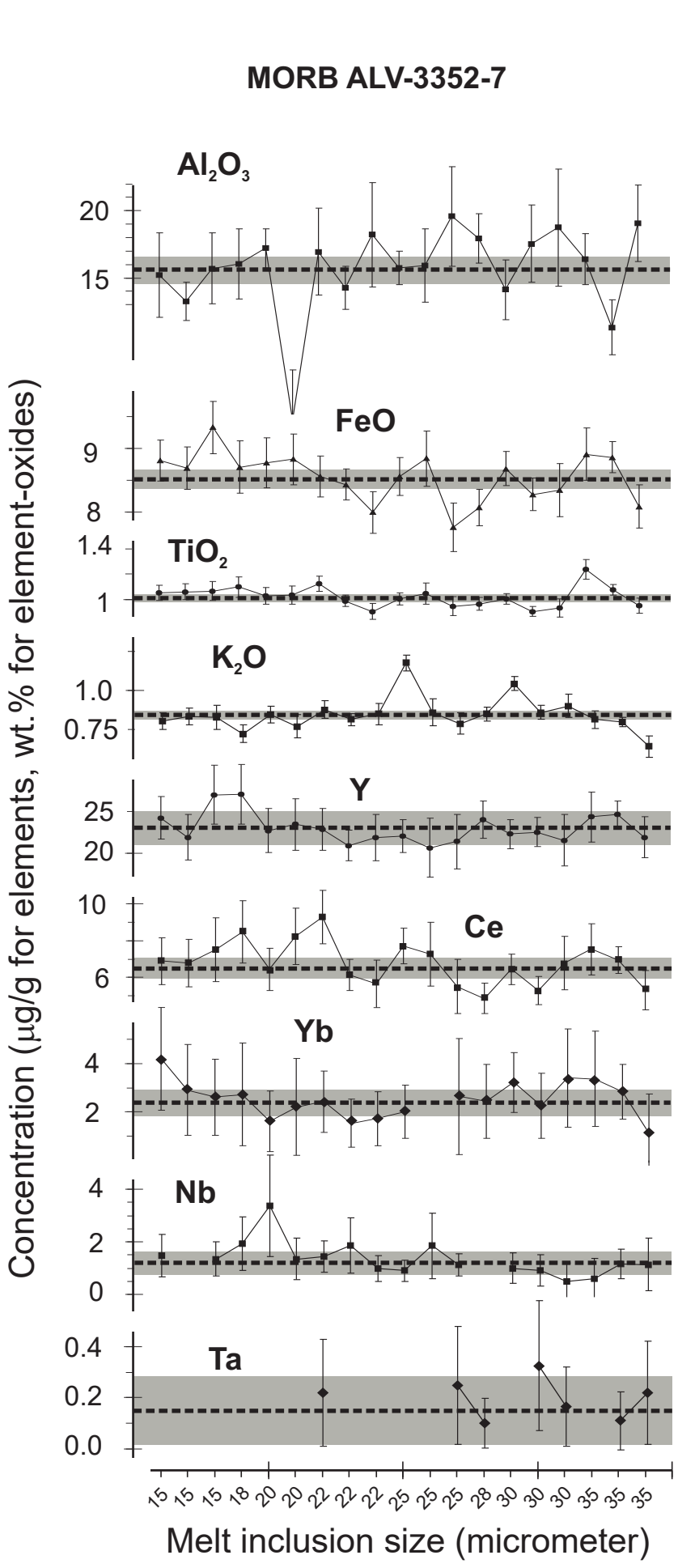
MORB ALV-3352-7
Al2O3
20
15
FeO
9
8
TiO2
1.4
1
K2O
1.0
0.75
Y
25
20
Ce
10
6
Yb
4
2
Nb
4
2
0
Ta
0.4
0.2
0.0
Concentration (μg/g for elements, wt.% for element-oxides)
15 15 15 18 20 20 22 22 22 25 25 25 28 30 30 30 35 35 35
Melt inclusion size (micrometer)

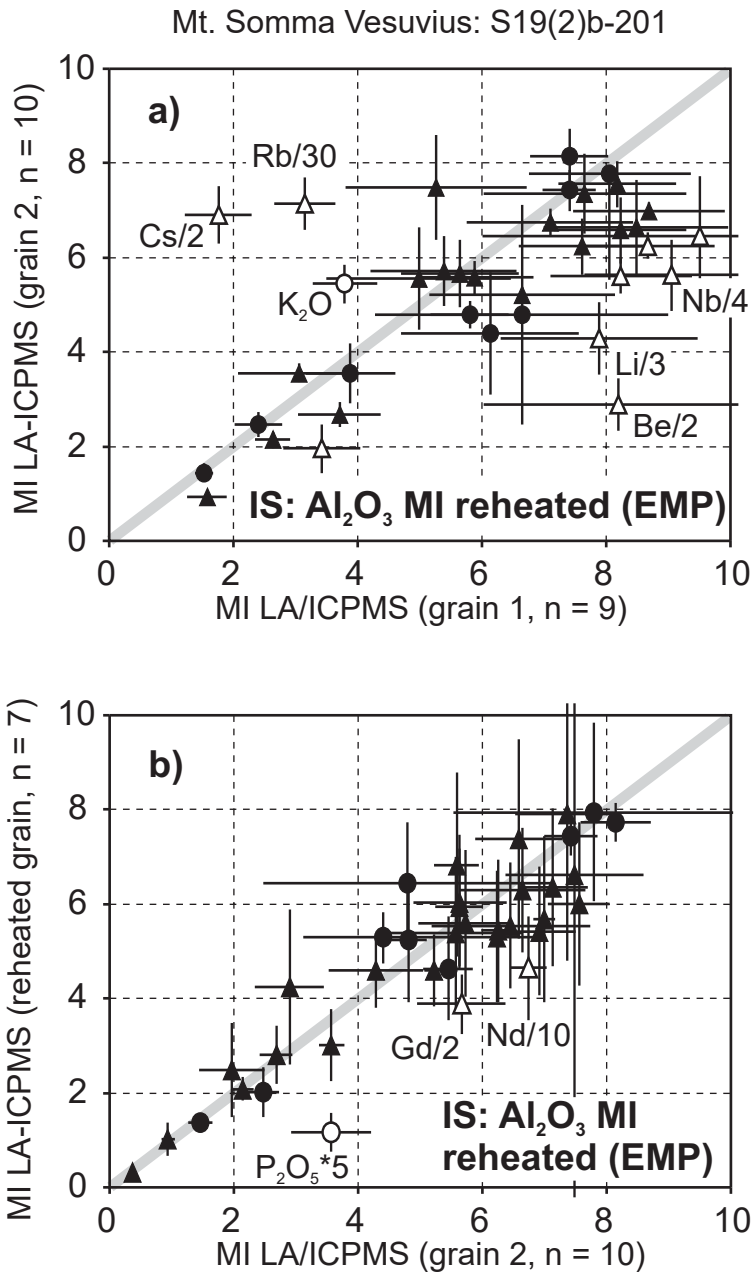
Mt. Somma Vesuvius: S19(2)b-201
a)
Rb/30
Cs/2
K2O
Nb/4
Li/3
Be/2
IS: Al2O3 MI reheated (EMP)
MI LA-ICPMS (grain 2, n = 10)
MI LA/ICPMS (grain 1, n = 9)
b)
Gd/2
Nd/10
P2O5*5
IS: Al2O3 MI reheated (EMP)
MI LA-ICPMS (reheated grain, n = 7)
MI LA/ICPMS (grain 2, n = 10)

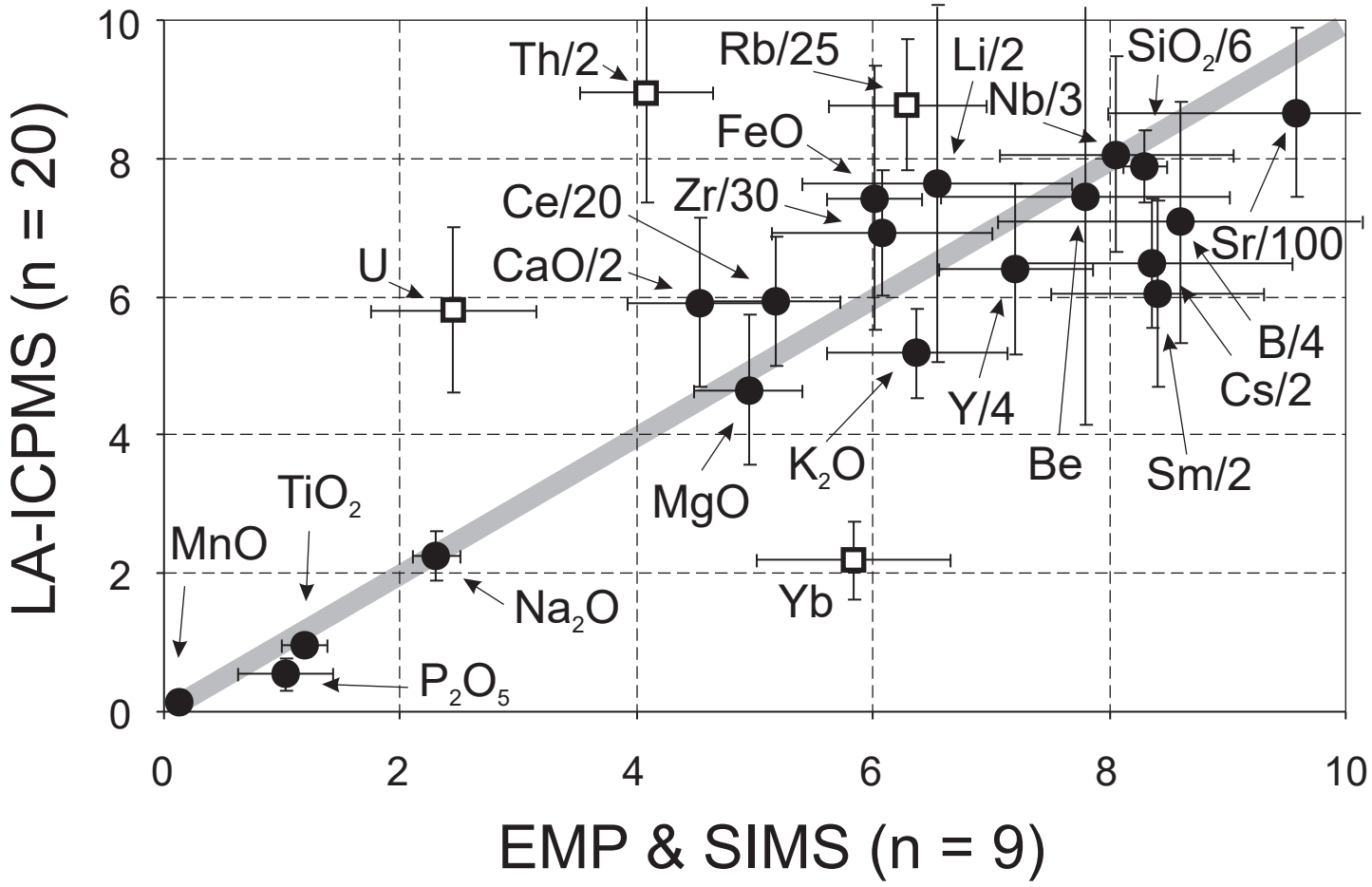
LA-ICPMS (n = 20)
EMP & SIMS (n = 9)
0
2
4
6
8
10
Th/2
Rb/25
Li/2
Nb/3
SiO2/6
FeO
Ce/20
Zr/30
Sr/100
U
CaO/2
B/4
Cs/2
Y/4
K2O
Be
Sm/2
MgO
TiO2
MnO
Na2O
Yb
P2O5

Table 1: LA-ICPMS instrument and data acquisition parameters

Excimer 193 nm ArF laser Compex 110I

- Output energy	70 - 100 mJ
- Energy density on sample	10 - 15 J/cm^2, homogeneous energy distribution
- Pulse duration	15 ns
- Repetition rate	10 Hz
- Pit sizes	Between 8 and 80 µm
- Ablation cell volume	1 cm^3
- Cell gas flow	0.9 - 1.0 l min^{-1} He

ELAN 6100 quadrupole ICP-MS

- Nebulizer gas flow	0.80 - 0.90 l min^{-1} Ar
- Auxiliary gas flow	0.75 - 0.90 l min^{-1} Ar
- Cool gas flow	13.0 - 15.0 l min^{-1} Ar
- rf power	1200 - 1300 kV
- Detector mode	Dual, 8 orders of magnitude linear dynamic range
- Quadrupole settling time	3 ms
- Detector housing vacuum	1.5 - 2.8 *10^{-5} Torr during analysis

Data acquisition parameters

- Sweeps per reading	1
- Readings per replicate	200 - 300
- Replicates	1
- Dwell time per isotope	10 ms
- Points per peak	1 per measurement
- Oxide production rate	Tuned to <0.2% ThO
- Isotopes analyzed	^{7}Li, ^{9}Be, ^{11}B, ^{23}Na, ^{25}Mg ^{27}Al, ^{29}Si, ^{31}P, ^{39}K, ^{42}Ca, ^{45}Sc, ^{49}Ti, ^{51}V, ^{53}Cr, ^{55}Mn, ^{57}Fe, ^{59}Co, ^{62}Ni, ^{66}Zn, ^{85}Rb, ^{88}Sr, ^{89}Y, ^{91}Zr, ^{93}Nb, ^{133}Cs, ^{137}Ba, ^{139}La, ^{140}Ce, ^{141}Pr, ^{146}Nd, ^{147}Sm, ^{153}Eu, ^{157}Gd, ^{159}Tb, ^{163}Dy, ^{165}Ho, ^{167}Er, ^{169}Tm, ^{173}Yb, ^{175}Lu, ^{178}Hf, ^{181}Ta, ^{208}Pb, ^{232}Th, ^{238}U

Table 2: LA-ICPMS, EMP and SIMS data of MORB sample ALV-3352-7

		Plagioclase host				Matrix Glass						MI exposed		Whole MI					Whole MI		Whole MI		Whole MI	
		EMP		LA-ICP-MS		EMP		LA-ICPMS		SIMS		EMP		LA-ICPMS					LA-ICPMS		LA-ICPMS		LA-ICPMS	
		n = 50		n = 17		n = 20		n = 20		n = 7		n = 6		n = 19					n=19		n = 19		n = 19	
		aver [A]	1SD [A]	aver [A]	1SD [A]	aver [A]	1SD [A]	aver [A]	1SD [A]	aver [A]	1SD [A]	aver [A]	1SD [A]	aver [A]	1SD [A]	wt-av [A]	1SD [A]	MSWD [A]	aver [A]	1SD [A]	aver [A]	1SD [A]	aver [A]	1SD [A]
SiO2	wt-%	48.0	1.4	48.9	6.1	50.2	0.1	51.2	4.2			50.2	0.1	50.2	4.0	50.8	1.1	0.6	49.8	4.5	50.2	3.8	50.2	3.6
TiO2	wt-%	0.039	0.014	0.028	0.007	1.33	0.05	1.15	0.03	1.20	0.02	1.30	0.04	1.02	0.08	1.01	0.01	1.8	1.13	0.09	0.98	0.08	0.92	0.07
Al2O3	wt-%	32.5	0.9	**32.5** [B]	**0.9**	15.2	0.1	15.7	1.2			13.9	0.01	15.7	3.4	15.6	0.5	1.1	14.5	2.5	16.9	2.1	17.3	3.0
Cr2O3	wt-%	na		na		0.050	0.025	0.052	0.002			0.060	0.007	0.051	0.006	0.052	0.003	0.2	0.057	0.006	0.049	0.005	0.046	0.005
FeO	wt-%	0.427	0.075	0.413	0.053	9.14	0.10	8.96	0.85			9.63	0.12	8.55	0.39	8.52	0.07	1.2	9.46	0.43	8.23	0.37	7.76	0.35
MnO	wt-%	0.012	0.004	0.005	0.001	0.177	0.046	0.173	0.009			0.165	0.028	0.173	0.004	0.173	0.001	0.3	0.191	0.005	0.166	0.004	0.156	0.004
NiO	wt-%	na		na		0.010	0.006	na				na		na		na			na		na		na	
MgO	wt-%	0.239	0.042	0.264	0.048	8.16	0.04	7.95	0.73			9.42	0.06	**8.48** [D]		**8.48**			**9.42** [E]	**0.06**	**8.16** [F]	**0.04**	**7.68** [G]	**0.04**
CaO	wt-%	16.3	1.0	15.1	0.6	12.4	0.1	12.0	0.5			11.9	0.2	13.3	2.7	12.7	0.3	2.7	12.9	3.0	13.4	2.5	13.5	2.3
Na2O	wt-%	1.99	0.51	2.17	0.87	2.47	0.05	2.68	0.40			2.18	0.05	2.55	0.28	2.57	0.04	1.9	2.57	0.34	2.52	0.26	2.48	0.23
K2O	wt-%	0.012	0.008	0.011	0.004	0.077	0.021	0.084	0.004			0.093	0.014	0.085	0.011	0.085	0.001	4.6	0.093	0.013	0.082	0.011	0.077	0.010
P2O5	wt-%	na		na		0.097	0.012	na				0.103	0.021	na		na			na		na		na	
Total	wt-%	99.5		99.4		99.1		**100.0** [C]				98.8							100.1		100.0		92.4	
Li	(µg/g)			1.4	0.6			6.2	1.7	na														
Be	(µg/g)			na				4.2	3.5	na														
Sc	(µg/g)			0.85	0.17			41	1	na				41	4	40	2	0.4	45.6	4.8	39.1	4.1	36.8	3.9
Rb	(µg/g)			0.43	0.40			0.89	0.11	na				1.0	0.5	0.70	0.14	0.5	1.1	0.6	0.97	0.50	0.90	0.49
Sr	(µg/g)			156	11			99	1	97	1			97	19	95	3	2.5	91.8	28.1	98.7	22.7	101	21
Y	(µg/g)			0.18	0.04			25	1	na				23	2	23	1	0.4	25.6	2.0	22.1	1.7	20.8	1.6
Zr	(µg/g)			0.17	0.12			67	1	69	1			59	8	56	1	1.5	65.2	9.1	56.5	7.8	53.1	7.4
Nb	(µg/g)			0.20	0.16			1.5	0.1	na				1.4	0.7	1.2	0.2	0.3	1.5	0.7	1.4	0.6	1.2	0.6
Cs	(µg/g)			0.20	0.20			0.11	0.10	na				na		na			na		na		na	
Ba	(µg/g)			1.4	0.4			6.5	0.3	na				5.9	2.2	5.2	0.7	0.5	6.4	2.5	6.0	2.3	0.5	2.1
La	(µg/g)			0.14	0.06			2.5	0.1	2.7	0.1			2.1	0.5	2.0	0.1	0.5	2.3	0.6	1.9	0.5	1.8	0.5
Ce	(µg/g)			0.44	0.29			7.8	0.2	7.9	0.1			6.8	1.2	6.5	0.3	1.0	7.4	1.3	6.5	1.1	6.2	1.1
Pr	(µg/g)			0.09	0.07			1.3	0.1	na				1.2	0.3	1.2	0.1	0.7	1.4	0.4	1.2	0.3	1.1	0.3
Nd	(µg/g)			0.23	0.09			7.7	0.3	6.6	0.5			6.6	1.5	6.3	0.5	0.4	7.0	1.8	6.3	1.5	6.0	1.4
Sm	(µg/g)			0.17	0.15			2.8	0.2	3.1	0.1			2.5	0.6	2.3	0.3	0.2	2.7	0.6	2.4	0.5	2.2	0.5
Eu	(µg/g)			0.23	0.06			1.1	0.1	1.0	0.1			1.3	0.4	1.2	0.1	0.3	1.4	0.4	1.3	0.4	1.2	0.3
Gd	(µg/g)			0.20	0.11			3.6	0.2	na				2.9	1.0	2.6	0.4	0.4	3.0	1.1	2.7	0.9	2.6	0.9
Tb	(µg/g)			0.03	0.03			0.70	0.03	na				0.62	0.13	0.57	0.07	0.2	0.55	0.12	0.59	0.13	0.56	0.12
Dy	(µg/g)			0.10	0.07			4.6	0.2	4.0	0.4			4.3	0.8	4.1	0.3	0.3	4.8	0.9	4.1	0.8	3.9	0.7
Ho	(µg/g)			0.07	0.06			1.0	0.1	na				0.91	0.27	0.88	0.08	0.3	0.99	0.30	0.88	0.26	0.83	0.24
Er	(µg/g)			0.07	0.02			2.8	0.2	3.0	0.2			2.4	0.7	2.1	0.3	0.5	2.7	0.7	2.3	0.6	2.1	0.6
Tm	(µg/g)			0.03	0.03			0.41	0.03	na				0.35	0.11	0.34	0.05	0.2	0.38	0.12	0.35	0.09	0.32	0.10
Yb	(µg/g)			0.12	0.11			2.9	0.2	2.5	0.2			2.5	0.8	2.3	0.3	0.2	2.8	0.9	2.4	0.7	2.3	0.7
Lu	(µg/g)			0.03	0.02			0.42	0.03	na				0.35	0.09	0.31	0.06	0.1	0.39	0.10	0.34	0.09	0.31	0.10
Hf	(µg/g)			0.08	0.04			1.9	0.1	na				1.3	0.5	1.1	0.2	0.4	1.4	0.6	1.3	0.5	1.2	0.5
Ta	(µg/g)			0.07	0.06			0.10	0.02	na				0.20	0.08	0.13	0.06	0.2	0.22	0.09	0.19	0.07	0.18	0.07
Pb	(µg/g)			0.84	0.73			0.87	0.79	na				6.0	5.9	2.6	0.4	6.6	3.0	2.1	2.8	1.7	5.6	9.0
Th	(µg/g)			0.07	0.05			0.11	0.02	na				0.23	0.23	0.15	0.06	0.6	0.28	0.26	0.24	0.21	0.22	0.21
U	(µg/g)			0.22	0.16			0.12	0.10	na				0.25	0.21	0.10	0.04	0.8	0.27	0.23	0.24	0.20	0.23	0.19

For each grain, the number of analyzed MI is given as n = value.

Note, however, that significant numbers were not always obtained for all trace elements, and concentrations represent the average of significant determinations as reported in the appendix.

[A] aver refers to average, wt-av refers to error-weighted average. 1SD refers to the absolute 1 standard deviation uncertainty. MSWD calculated on the basis of 1 SD.

[B] Al_2O_3 from EMP as internal standard

[C] 100 wt-% element oxides as internal standard

[D] MgO obtained from petrogenetic modeling as internal standard (see text for details)

[E] MgO from EMP of exposed MI as internal standard

[F] MgO from EMP of matrix glass as internal standard

[G] MgO from LA-ICPMS (n=4) of fused whole rock glass as internal standard

na not analysed

Table 3: LA-ICPMS, SIMS and EMP data of melt inclusions of sample S19(2)b-201 from the 79 AD pumice horizon of Mt. Somma-Vesuvius

LA-ICPMS		Grain 1 (n = 9)		Grain 2 (n = 10)		Grain 5 (n = 2)		Reheated grain (n = 7)		All grains (n = 29)		Grain 2, 4, 5 and reheated (n = 20)					SIMS + EMP (n = 9)	
		aver [A]	1SD [A]	aver [A]	1SD [A]	aver [A]	1SD [A]	aver [A]	1SD [A]	aver [A]	1SD [A]	aver [A]	1SD [A]	wt-av [A]	2SD [A]	MSWD	aver [A]	1SD [A]
SiO2	wt-%	44.5	3.7	48.8	3.4	51.3	2.9	46.2	2.5	46.1	3.7	47.3	3.1	48.2	0.9	0.4	49.8	1.1
TiO2	wt-%	1.162	0.126	0.960	0.058	0.850	0.083	1.046	0.264	1.019	0.173	0.962	0.165	0.993	0.014	4.6	1.188	0.192
Al2O3 [B]	wt-%	14.8	0.9	14.8	0.9	14.8	0.9	14.8	0.9	14.8	0.9	14.8	0.9				14.8	0.9
FeO	wt-%	8.07	1.31	7.78	2.24	6.43	1.91	7.91	1.89	7.58	1.73	7.42	1.91	7.63	0.11	8.8	6.01	0.41
MnO	wt-%	0.152	0.014	0.146	0.019	0.131	0.016	0.137	0.021	0.142	0.018	0.139	0.020	0.145	0.002	3.8	0.133	0.033
MgO	wt-%	6.14	1.43	4.39	1.28	5.56	1.01	5.27	0.53	5.09	1.34	4.66	1.09	4.72	0.23	0.8	4.95	0.46
CaO	wt-%	13.29	4.72	9.56	4.63	7.83	4.80	12.83	2.58	12.84	2.94	11.83	2.44	10.46	0.40	3.6	9.08	1.24
Na2O	wt-%	2.39	0.39	2.46	0.26	2.30	0.30	2.01	0.52	2.28	0.36	2.26	0.35	2.30	0.01	63	2.31	0.20
K2O	wt-%	3.79	0.52	5.44	0.40	5.12	0.59	4.61	1.10	4.71	0.91	5.18	0.64	5.28	0.02	115	6.37	0.77
P2O5	wt-%	0.776	0.145	0.711	0.128	0.652	0.173	0.233	0.081	0.615	0.230	0.546	0.234	0.342	0.003	240	1.033	0.403
Volatiles [C]	wt-%	5		5		5		5		5		5		5			4.9	1.6
Li	(µg/g)	24	5	13	2	17	3	14	2	17	6	15	5	15	1	2.0	13.1	2.3
Be	(µg/g)	16	4	5.8	1.1	nd		8.5	3.3	9.3	5.0	7.5	3.3	6.4	1.4	0.9	7.8	1.2
B	(µg/g)	33	4	26	3	23	4	29	8	29	7	28	7	28	2	1.2	34.4	6.2
Sc	(µg/g)	26	7	37	6	nd		33	40	37	19	40	20	33	3	1.9	na	
V	(µg/g)	370	67	268	27	275	42	280	60	292	64	270	46	283	6	2.8	na	
Cr	(µg/g)	297	36	nd		nd		351	381	292	193	293	303	170	23	4.9	na	
Co	(µg/g)	38	8	37	4	26	7	39	15	36	11	36	12	39	2	2.7	na	
Ni	(µg/g)	204	191	25	12	nd		166	163	96	74	71	53	106	16		na	
Zn	(µg/g)	100	22	78	2	56	8	69	11	76	19	70	12	76	3	0.5	na	
Rb	(µg/g)	94	15	214	17	237	31	190	50	177	64	219	24	219	1	34	157	17
Sr	(µg/g)	1238	171	842	58	841	32	887	186	978	214	866	122	883	5	21	958	158
Y	(µg/g)	34	6	27	4	22	2	25	5	28	6	26	5	27	1	4.8	28.8	2.6
Zr	(µg/g)	263	28	215	16	168	3	208	26	224	36	208	27	211	2	13	182	28
Nb	(µg/g)	36	6	23	3	27	1	24	6	28	7	24	4	25.1	0.3	6.0	24.2	3.0
Ba	(µg/g)	2177	306	1747	44	1356	131	1414	434	1692	395	1556	315	1568	9	57	na	
Cs	(µg/g)	3.5	1.1	14	1	14	3	11	3	9.9	4.8	13	2	12.9	0.2	5.0	16.7	2.4
La	(µg/g)	87	11	62	3	58	4	54	15	66	15	60	11	61	1	11	na	
Ce	(µg/g)	152	20	124	12	106	3	106	28	128	24	119	19	123	1	20	103	11
Nd	(µg/g)	71	13	67	3	47	2	46	11	59	13	56	11	59	1	3.7	na	
Sm	(µg/g)	19	7	13	3	11.3	0.3	11	3	14	5	12	3	13	1	0.9	16.8	1.8
Eu	(µg/g)	3.0	1.0	3.6	0.2	nd		3.0	0.8	3.2	0.7	3.2	0.7	3.2	0.2	0.5	na	
Gd	(µg/g)	11	2	11	1	8.0	0.9	7.7	1.2	9.7	2.1	9.3	2.1	9.6	0.6	0.7	na	
Yb	(µg/g)	3.4	0.6	2.0	0.5	nd		2.5	1.0	2.5	0.8	2.2	0.6	2.2	0.3	0.2	5.8	0.8
Lu	(µg/g)	0.51	0.18	0.37	0.06	0.32	0.04	0.31	0.08	0.35	0.08	0.34	0.07	0.36	0.04	0.5	na	
Hf	(µg/g)	5.9	0.9	5.6	0.4	3.5	1.4	6.8	1.9	5.7	1.4	5.7	1.5	5.9	0.3	1.3	na	
Ta	(µg/g)	1.6	0.3	0.94	0.11	nd		1.0	0.3	1.2	0.3	1.0	0.2	1.1	0.1	2.0	na	
Pb	(µg/g)	33	4	30	2	36	7	24	7	30	5	29	5	26.6	0.4	48	na	
Th	(µg/g)	16	4	17	2	22	3	17	5	17	3	18	3	18.3	0.2	1459	8.2	1.1
U	(µg/g)	5.0	1.5	5.6	1.1	7.1	0.8	5.4	1.6	5.5	1.3	5.8	1.2	5.9	0.1	466	2.5	0.7

For each grain, the amount of analyzed MI is given as n = value.
Note, however, that significant numbers were not always obtained for all trace elements, and concentrations are the average of significant determinations as reported in the appendix.

[A] aver refers to average, wt-av refers to error-weighted average. 1SD and 2 SD refers to the absolute 1 and 2 standard deviation uncertainties, respectively

[B] Average EMP value used as an IS for the quantification of LA-ICPMS signals

[C] Volatiles are the sum of H_2O + F + SO_2 + Cl, set to 5.0 wt-% for quantification of LA-ICPMS signals

MSWD MSWD based on 2 standard deviation uncertainties on single MI analyses (Halter et al., 2002b)

nd not detected

na not analysed

Table 4: LA-ICPMS and EMP data of clinopyroxene grains of sample S19(2)b-201 from the 79 AD pumice horizon of Mt. Somma-Vesuvius

		Grain 1				Grain 2				Grain 5		Reheated grain			
		LA-ICPMS n = 12		EMP n = 33		LA-ICPMS n = 14		EMP n = 36		LA-ICPMS n = 3		LA-ICPMS n = 10		EMP n = 17	
		aver [A]	1 SD [A]	aver [A]	1 SD [A]	aver [A]	1 SD [A]	aver [A]	1 SD [A]	aver [A]	1 SD [A]	aver [A]	1 SD [A]	aver [A]	1 SD [A]
SiO2	wt-%	51.8	1.4	50.6	2.0	53.3	0.9	53.7	1.0	52.8	1.2	51.3	1.3	51.4	2.0
TiO2	wt-%	0.737	0.062	0.900	0.130	0.446	0.027	0.520	0.070	0.435	0.078	0.768	0.089	1.070	0.200
Al2O3	wt-%	5.03	0.46	4.91	0.77	2.84	0.20	2.71	0.46	2.96	0.70	4.71	0.69	5.70	1.20
FeO	wt-%	6.84	0.27	6.70	0.24	5.72	0.45	5.26	0.67	4.13	0.09	6.12	0.93	7.06	0.95
MnO	wt-%	0.138	0.004	0.130	0.020	0.099	0.004	0.090	0.030	0.090	0.004	0.110	0.008	0.100	0.030
MgO	wt-%	14.0	0.4	13.8	0.4	14.9	0.3	15.0	0.7	16.1	0.4	13.9	1.2	12.6	1.0
CaO	wt-%	21.1	1.1	22.6	0.2	22.4	0.9	23.7	0.2	23.3	1.0	23.3	0.8	23.7	17.0
Na2O	wt-%	0.361	0.022	0.340	0.130	0.225	0.016	0.180	0.050	0.189	0.015	0.262	0.031	0.230	0.030
K2O	wt-%	0.016	0.013	0.013	0.020	0.016	0.018	0.006	0.011	0.002	0.000	0.015	0.012	0.006	0.006
P2O5	wt-%	0.026	0.004	0.039	0.018	0.008	0.002	0.017	0.020	0.008	0.001	0.010	0.002	0.020	0.018
Mg-#		0.78		0.79		0.82		0.84		0.87		0.80		0.76	
Li	(µg/g)	2.3	0.6			1.5	0.5			1.8	0.2	1.7	0.5		
Be	(µg/g)	<1				<1				<1		1.2	0.2		
B	(µg/g)	<2				<2				<2		1.6	0.4		
Sc	(µg/g)	80.1	1.7			99.4	4.5			89.4	4.7	111	25		
V	(µg/g)	291	10			231	8			158	18	242	30		
Cr	(µg/g)	427	50			12.9	3.6			772	5	421	281		
Co	(µg/g)	41.1	2.2			54.8	2.1			32.8	1.1	39.1	4.6		
Ni	(µg/g)	125	11			17.5	2.5			151	12	94.0	26.1		
Zn	(µg/g)	34.6	3.3			22.9	0.7			18.8	0.8	27.6	6.7		
Rb	(µg/g)	0.62	0.47			0.88	0.50			<0.1		0.62	0.49		
Sr	(µg/g)	200	14			100	7			105	9	133	19		
Y	(µg/g)	22.1	2.2			6.9	0.7			7.3	0.3	14.3	1.5		
Zr	(µg/g)	102	12			20.4	3.8			17.0	0.3	70.8	16.9		
Nb	(µg/g)	0.57	0.14			0.10	0.05			0.067	0.011	0.33	0.10		
Ba	(µg/g)	3.4	1.9			6.3	4.2			0.38	0.23	3.4	2.7		
Cs	(µg/g)	0.027	0.004			0.097	0.042			<0.04		0.064	0.019		
La	(µg/g)	11.6	0.8			2.6	0.2			3.8	0.7	7.6	0.7		
Ce	(µg/g)	39.0	3.4			10.2	1.0			13.2	2.6	25.0	2.9		
Nd	(µg/g)	36.0	1.9			10.7	1.1			13.4	2.9	22.5	2.4		
Sm	(µg/g)	8.8	1.5			3.3	0.4			4.0	0.8	6.3	0.7		
Eu	(µg/g)	2.7	0.2			0.74	0.02			1.1	0.1	1.7	0.2		
Gd	(µg/g)	8.0	1.3			2.5	0.5			3.2	0.7	5.0	0.7		
Yb	(µg/g)	1.5	0.3			0.56	0.16			0.49	0.14	1.1	0.2		
Lu	(µg/g)	0.24	0.04			0.060	0.020			0.086	0.016	0.15	0.03		
Hf	(µg/g)	4.1	0.8			1.2	0.2			1.1	0.2	3.1	0.8		
Ta	(µg/g)	0.086	0.025			0.010	0.005			0.018	0.008	0.055	0.018		
Pb	(µg/g)	0.69	0.16			0.52	0.13			0.42	0.06	0.43	0.08		
Th	(µg/g)	0.31	0.07			0.087	0.061			0.10	0.03	0.18	0.05		
U	(µg/g)	0.083	0.047			0.029	0.015			0.011	0.003	0.065	0.048		

A aver refers to average, 1SD to the absolute 1 standard deviation uncertainty of n spot analyses

Mg-# The magnesium number, calculated as molar (Mg/(Mg+Fe), whereby molar Fe is based on total Fe expressed as FeO

Appendix A. LA-ICPMS data of individual melt inclusions of MORB sample ALV-3352-7, East Pacific Rise

	MI size	SiO_2		TiO_2		Al_2O_3		FeO		MnO		MgO[a]		CaO		Na_2O		K_2O	
	(μm)	(wt.%)	2SD	(wt.%)	2SD	(wt.%)	2SD	(wt.%)	2SD	(wt.%)	2SD	(wt.%)	2SD	(wt.%)	2SD	(wt.%)	2SD	(wt.%)	2SD
st07a03	20	47.6	3.5	1.03	0.06	17.2	1.4	8.8	0.4	0.172	0.008	8.48		14.3	1.1	2.4	0.1	0.085	0.005
st07a04	15	55.8	6.0	1.05	0.06	15.2	3.1	8.8	0.3	0.180	0.006	8.48		7.8	4.9	2.6	0.2	0.080	0.005
st07a05	25	50.6	3.0	1.00	0.05	15.7	1.3	8.6	0.3	0.170	0.006	8.48		12.8	0.9	2.5	0.1	0.118	0.005
st07a06	35	48.4	4.3	1.23	0.08	16.4	1.9	8.9	0.4	0.177	0.008	8.48		14.0	1.4	2.3	0.2	0.081	0.006
st07a07	25	51.0	7.2	1.05	0.08	15.9	2.7	8.8	0.4	0.174	0.009	8.48		11.9	2.0	2.5	0.2	0.086	0.009
st07a09	22	47.6	6.7	1.12	0.06	17.0	3.2	8.6	0.3	0.171	0.006	8.48		14.6	2.1	2.4	0.2	0.088	0.006
st07a11	22	55.5	3.5	0.99	0.04	14.3	1.6	8.4	0.2	0.171	0.005	8.48		9.5	1.1	2.6	0.1	0.081	0.004
st07a12	15	56.4	3.7	1.06	0.06	13.2	1.4	8.7	0.3	0.172	0.007	8.48		9.3	1.1	2.5	0.1	0.083	0.005
st07a13	30	54.6	4.3	1.00	0.04	14.1	2.2	8.7	0.3	0.173	0.005	8.48		10.1	1.4	2.8	0.2	0.104	0.004
st07b03	15	50.3	6.9	1.06	0.08	15.7	2.6	9.3	0.4	0.182	0.008	8.48		12.0	1.9	2.9	0.2	0.083	0.008
st07b05	8	46.4	5.0	1.10	0.08	16.0	2.6	8.7	0.4	0.166	0.008	8.48		16.5	1.7	2.5	0.2	0.072	0.006
st07b06	35	52.8	3.7	1.07	0.04	11.3	2.0	8.9	0.2	0.175	0.005	8.48		14.3	1.1	3.0	0.1	0.080	0.003
st07b08	20	56.6	10.0	1.03	0.07	*4.4*	*3.7*	8.8	0.4	0.176	0.008	8.48		17.1	3.0	3.3	0.3	0.077	0.007
st07c07	30	47.2	5.5	0.90	0.04	17.5	2.9	8.3	0.3	0.173	0.005	8.48		14.9	1.7	2.5	0.2	0.086	0.004
st07c08	35	46.8	5.7	0.95	0.06	19.1	2.9	8.1	0.3	0.167	0.007	8.48		14.1	1.8	2.2	0.2	0.064	0.007
st07c09	22	47.6	7.5	0.90	0.06	18.2	3.9	8.0	0.3	0.167	0.007	8.48		14.2	2.4	2.3	0.3	0.085	0.007
st07c11	25	46.5	7.2	0.94	0.07	19.6	3.7	7.8	0.4	0.172	0.008	8.48		14.2	2.3	2.3	0.3	0.079	0.007
st07c12	28	48.4	4.0	0.96	0.05	17.9	1.8	8.1	0.3	0.170	0.006	8.48		13.6	1.2	2.4	0.2	0.085	0.004
st07c14	30	43.3	7.8	0.93	0.07	18.7	4.3	8.3	0.4	0.172	0.008	8.48		17.7	4.7	2.3	0.3	0.090	0.007

	MI size	La		Ce		Pr		Nd		Sm		Eu		Gd		Tb		Dy	
	(μm)	(μg/g)	2SD	(μg/g)	2SD	(μg/g)	2SD	(μg/g)	2SD	(μg/g)	2SD	(μg/g)	2SD	(μg/g)	2SD	(μg/g)	2SD	(μg/g)	2SD
st07a03	20	2.1	0.7	6.4	1.1	1.0	0.4	6.5	2.4	1.7	1.4	1.3	0.7	4.2	2.1	0.7	0.4	4.8	1.7
st07a05	25	1.9	0.5	7.7	0.9	1.4	0.3	6.9	1.9	1.5	1.0	0.7	0.4	4.2	1.6	0.5	0.2	4.6	1.3
st07a06	35	2.4	0.8	7.5	1.4	1.6	0.6	7.1	2.8	2.4	1.6	0.8	0.6	2.8	2.1	0.7	0.4	4.2	1.8
st07a07	25	2.3	0.9	7.3	1.7	1.3	0.7	8.3	3.4	<3.5		2.2	1.1	<5.3		0.6	0.4	4.5	2.1
st07a09	22	< 1.0		9.3	1.4	0.6	0.6	8.2	2.8	3.0	1.4	0.9	0.9	2.8	1.5	0.7	0.3	5.1	1.8
st07a11	22	2.2	0.5	6.1	0.9	1.0	0.3	6.5	1.8	2.1	1.2	1.3	0.5	2.9	1.4	0.6	0.2	4.1	1.2
st07a12	15	2.1	0.7	6.8	1.3	1.8	0.6	3.7	2.3	2.7	2.1	1.3	0.7	2.7	2.0	0.8	0.4	5.6	2.1
st07a13	30	2.3	0.5	6.4	0.8	1.0	0.3	6.9	1.7	2.9	1.2	1.1	0.5	2.5	1.1	0.5	0.2	3.4	1.0
st07b03	15	2.3	1.1	7.5	1.7	1.2	0.5	4.9	3.6	3.0	1.9	1.2	0.7	2.5	1.4	0.4	0.3	5.3	2.1
st07b05	18	3.4	1.1	8.5	1.7	1.6	0.6	7.1	3.3	3.2	2.4	1.2	0.8	2.1	2.1	0.7	0.5	4.7	2.1
st07b06	35	2.5	0.4	7.0	0.7	1.7	0.3	7.9	1.6	2.7	1.0	1.3	0.4	3.3	1.1	0.7	0.2	4.2	0.9
st07b08	20	2.5	1.1	8.2	1.5	1.2	0.7	7.0	3.1	2.9	1.6	1.3	0.8	5.1	2.4	<1.0		4.5	1.8
st07c07	30	1.4	0.6	5.3	0.8	1.7	0.4	4.6	1.2	1.8	0.8	1.2	0.6	2.6	1.5	0.4	0.2	4.3	1.2
st07c08	35	2.2	0.7	5.3	1.1	1.5	0.4	5.0	2.4	2.6	2.0	<0.7		1.9	1.1	0.6	0.3	5.0	1.8
st07c09	22	1.4	0.6	5.7	1.3	1.1	0.5	9.0	3.7	2.4	2.8	0.9	0.5	1.4	0.9	0.6	0.3	2.8	1.2
st07c11	25	1.3	0.7	5.5	1.5	0.8	0.4	3.9	2.8	<6.7		1.6	1.1	1.7	1.8	0.7	0.4	2.7	1.7
st07c12	28	1.4	0.5	4.9	0.8	1.0	0.4	5.8	1.9	1.4	1.6	1.8	0.6	2.3	1.5	0.4	0.2	4.1	1.5
st07c14	30	1.8	0.8	6.8	1.4	1.0	0.5	7.5	3.2	2.3	2.1	1.8	0.9	<3.9		0.8	0.4	4.6	2.2

Italic values have not been considered for average calculations.

[a] The internal standard element concentration for the quantification of LA-ICPMS signals, derived from petrogenetic modelling as explained in the text.

[b] Volatiles are the sum of H2O+F+SO2+Cl, set to 0 wt.% for quantification of LA-ICPMS signals.

Appendix A (*continued*)

	Volatiles	Sc		Cr		Rb		Sr		Y		Zr		Nb		Ba		Cs	
	(wt.%)[b]	(μg/g)	2SD	(μg/g)	2SD	(μg/g)	2SD	(μg/g)	2SD	(μg/g)	2SD	(μg/g)	2SD	(μg/g)	2SD	(μg/g)	2SD	(μg/g)	2SD
st07a03	0	46	7	341	73	1.3	0.7	105	10	23	3	62	7	1.5	0.8	6	3	<0.17	
st07a04	0	38	7	411	84	<3.2		74	19	24	3	59	6	<3.1		<3.6		<0.70	
st07a05	0	38	5	347	56	<0.6		104	9	22	2	53	5	1.3	0.6	8	3	<0.39	
st07a06	0	39	7	338	79	0.7	0.6	116	14	24	3	77	8	1.9	1.0	5	3	<0.20	
st07a07	0	39	12	323	140	0.7	1.1	106	21	21	4	68	10	3.4	1.9	4	3	0.50	0.32
st07a09	0	33	6	331	85	1.9	1.1	114	21	23	3	62	6	1.4	0.8	8	4	<0.45	
st07a11	0	37	5	410	62	0.7	0.4	66	10	21	2	57	5	1.4	0.6	6	2	<0.26	
st07a12	0	39	8	335	84	0.9	0.7	61	11	22	3	57	7	1.9	1.0	4	3	<0.44	
st07a13	0	41	5	350	52	0.6	0.4	81	13	22	2	55	4	1.0	0.5	2	2	<0.26	
st07b03	0	48	10	267	180	<2.5		87	19	27	4	71	9	0.9	0.4	3	3	<1.04	
st07b05	0	39	9	339	99	0.4	0.6	128	16	27	4	69	9	1.9		9	5	<0.49	
st07b06	0	39	4	375	50	0.5	0.2	113	10	25	2	59	4	1.1		6	2	<0.16	
st07b08	0	34	8	369	103	<1.5		122	28	23	3	63	8	<2.9		7	6	<0.73	
st07c07	0	40	6	319	77	0.8	0.6	99	15	23	2	48	4	1.0	0.6	<2.3		<0.27	
st07c08	0	43	7	413	85	<0.7		77	16	22	2	45	6	0.9	0.6	<2.5		<0.29	
st07c09	0	44	9	302	73	<2.2		102	21	22	3	54	7	0.5	0.7	4	3	<0.51	
st07c11	0	40	9	321	108	1.3	0.9	89	20	21	3	55	8	0.6	0.8	7	5	<0.65	
st07c12	0	48	6	353	66	1.2	0.7	96	11	24	2	54	5	1.2	0.6	4	2	<0.34	
st07c14	0	47	9	382	101	2.2	1.2	110	23	22	3	50	7	1.1	1.0	10	5	<0.77	

	Ho		Er		Tm		Yb		Lu		Hf		Ta		Pb		Th		U	
	(μg/g)	2SD	(μg/g)	2SD	(μg/g)	2SD	(μg/g)	2SD	(μg/g)	2SD	(μg/g)	2SD	(μg/g)	2SD	(μg/g)	2SD	(μg/g)	2SD	(μg/g)	2SD
st07a03	0.6	0.3	2.5	1.3	0.4	0.2	1.6	1.3	0.4	0.3	0.9	0.8	<0.15		<1.4		<0.16		<0.25	
st07a04	0.8	0.4	1.8	1.3	<1.0		4.2	2.1	0.4	0.3	1.2	0.9	<0.96		<5.2		<0.73		<0.72	
st07a05	1.4	0.4	2.5	1.0	0.5	0.2	2.0	1.1	0.3	0.2	1.0	0.6	<0.25		<1.0		0.17	0.11	<0.25	
st07a06	0.9	0.4	2.5	1.5	0.4	0.3	3.4	2.0	0.5	0.4	2.4	1.3	<0.25		<1.9		0.70	0.35	0.50	0.31
st07a07	1.0	0.5	2.9	1.9	<1.5		<3.1		<0.8		1.2	1.3	<1.10		1.7	1.9	0.17	0.16	<0.66	
st07a09	1.1	0.4	0.7	0.7	<0.5		2.4	1.3	<0.6		1.2	0.9	0.22	0.21	1.1	1.6	<0.35		<0.80	
st07a11	0.9	0.3	2.8	1.0	0.3	0.2	1.5	1.0	0.3	0.2	1.7	0.7	<0.34		<1.9		0.17	0.14	<0.27	
st07a12	0.7	0.4	2.3	1.4	0.3	0.2	2.9	1.9	0.4	0.3	1.0	0.9	<0.54		<2.6		<0.39		<0.29	
st07a13	0.8	0.3	2.8	1.0	0.4	0.2	3.2	1.2	0.2	0.1	1.3	0.6	<0.42		<2.1		<0.29		<0.34	
st07b03	1.0	0.5	3.7	2.0	0.4	0.3	2.6	1.6	0.4		1.0	1.0	<0.95		<5.1		0.16	0.12	<0.75	
st07b05	1.5	0.6	3.1	1.9	0.4	0.3	2.7	2.1	0.5	0.4	1.9	1.2	<0.50		6.0	1.8	<0.52		0.13	0.12
st07b06	0.9	0.2	2.7	0.8	0.3	0.1	2.8	1.1	0.4	0.2	1.4	0.5	0.11	0.11	1.8	0.6	<0.18		0.06	0.06
st07b08	1.3	0.6	1.3	0.8	0.4	0.2	2.2	2.0	0.3	0.3	1.3	0.8	<1.78		1.5	1.2	0.15	0.12	<0.92	
st07c07	0.8	0.3	2.3	0.7	0.3	0.1	2.3	1.3	0.3	0.3	0.6	0.3	0.33	0.25	1.6	1.1	0.12		0.11	0.06
st07c08	0.7	0.5	2.7	1.6	0.5	0.3	1.1	1.6	0.2	0.2	1.3	1.0	0.22	0.20	<2.6		<0.15		<0.40	
st07c09	0.8	0.4	2.5	1.3	0.2	0.2	1.7	1.1	0.4	0.3	0.5	0.5	<0.43		5.4	1.3	<0.41		<0.66	
st07c11	0.5	0.5	2.1	1.5	0.1	0.3	2.6	2.4	0.3	0.3	1.2	1.0	0.25	0.23	4.3	2.1	<0.94		0.46	0.36
st07c12	0.7	0.4	2.2	1.1	0.5	0.2	2.4	1.5	0.2	0.2	1.1	0.5	0.10	0.10	2.9	2.5	<0.26		<0.12	
st07c14	0.8	0.4	1.7	1.5	0.2	0.3	3.4	2.0	<0.3		2.5	1.4	0.17	0.16	*33.7*	4.6	<0.70		<1.11	

Appendix B. A-ICPMS data of individual melt inclusions of sample S19(2)b-201, Mt. Somma-Vesuvius

	MI size	SiO_2		TiO_2		Al_2O_3[a]		FeO		MnO		MgO		CaO		Na_2O		K_2O		P_2O_5	
	(μm)	(wt.%)	2SD	(wt.%)	2SD	(wt.%)	2SD	(wt.%)	2SD	(wt.%)	2SD	(wt.%)	2SD	(wt.%)	2SD	(wt.%)	2SD	(wt.%)	2SD	(wt.%)	2SD
S19(2)d-2: MI crystallized (LA-ICPMS)																					
Grain 1																					
Al24a04	10	41.4	3.4	1.211	0.091	14.8		7.40	0.52	0.143	0.011	6.63	0.70	17.3	1.5	1.95	0.07	3.49	0.10	0.675	0.051
Al24a05	12	41.9	6.2	1.178	0.130	14.8		7.08	0.89	0.137	0.017	7.53	1.44	16.5	2.6	2.20	0.07	2.93	0.05	0.665	0.047
Al24a08	8	40.6	5.1	1.261	0.129	14.8		6.32	0.75	0.134	0.015	6.99	1.12	19.0	2.3	1.93	0.08	3.42	0.09	0.630	0.057
Al24a09	15	45.1	4.0	1.047	0.090	14.8		7.23	0.60	0.151	0.012	6.84	0.90	13.2	1.7	2.26	0.07	3.61	0.08	0.759	0.043
Al24a10	10	41.3	3.9	1.276	0.105	14.8		6.80	0.60	0.151	0.012	7.67	0.83	16.5	1.8	2.20	0.06	3.71	0.07	0.700	0.047
Al24b04	22	51.3	8.4	0.963	0.150	14.8		9.59	1.20	0.147	0.024	3.51	2.20	5.9	3.5	3.09	0.09	4.73	0.08	1.055	0.040
Al24b05	42	43.4	6.2	1.338	0.115	14.8		9.49	0.93	0.180	0.019	5.34	1.58	13.6	2.6	2.36	0.10	3.76	0.11	0.688	0.033
Al24b07	25	50.2	9.6	1.034	0.163	14.8		9.66	1.34	0.150	0.027	4.55	2.52	6.7	4.0	2.73	0.10	4.30	0.07	0.859	0.037
Al24b08	25	45.0	6.1	1.147	0.109	14.8		9.06	0.86	0.172	0.018	6.10	1.49	10.8	2.4	2.82	0.10	4.19	0.11	0.954	0.039
Grain 2																					
Al24a11	15	52.2	8.3	1.018	0.139	14.8		11.78	1.02	0.161	0.019	1.99	2.35	3.5	3.5	2.85	0.07	5.86	0.08	0.865	0.054
Al24a12	22	54.4	5.0	0.871	0.065	14.8		10.03	0.60	0.179	0.011	2.53	1.35	2.3	2.3	2.92	0.05	6.10	0.07	0.939	0.024
Al24a13	12	45.7	5.2	0.880	0.093	14.8		4.53	0.64	0.118	0.012	6.11	1.16	15.3	2.3	2.06	0.06	4.76	0.10	0.735	0.055
Al24a14	14	50.8	2.4	0.913	0.049	14.8		7.78	0.31	0.129	0.006	4.16	0.49	7.8	1.0	2.44	0.04	5.56	0.08	0.680	0.035
Al24a16	22	50.6	4.7	0.983	0.063	14.8		9.31	0.52	0.147	0.010	5.25	1.25	5.5	2.0	2.37	0.05	5.36	0.08	0.730	0.026
Al24a17	10	46.7	6.7	0.912	0.125	14.8		4.78	0.86	0.117	0.016	5.60	1.47	13.4	3.0	2.44	0.07	5.52	0.10	0.748	0.065
Al24b10	48	47.8	2.7	0.977	0.034	14.8		7.27	0.33	0.151	0.006	4.33	0.66	11.2	1.1	2.41	0.04	5.52	0.08	0.621	0.012
Al24b11	35	47.7	4.4	0.988	0.056	14.8		7.45	0.54	0.144	0.010	4.52	1.10	10.9	1.8	2.45	0.06	5.43	0.10	0.569	0.017
Al24b12	35	47.7	3.3	1.053	0.043	14.8		7.88	0.42	0.158	0.007	4.46	0.77	10.7	1.2	2.39	0.05	5.11	0.10	0.666	0.018
Al24b13	30	44.2	6.4	1.000	0.064	14.8		6.85	1.05	0.153	0.015	4.94	1.63	15.1	2.3	2.28	0.05	5.11	0.08	0.547	0.016
Grain 4																					
Al24b15	60	45.3	4.2	1.226	0.046	14.8		7.27	0.34	0.155	0.008	5.84	1.14	13.1	1.8	1.86	0.04	4.85	0.09	0.634	0.015
Grain 5																					
Al24b16	22	53.3	7.7	0.907	0.085	14.8		7.76	0.66	0.142	0.014	4.84	2.16	4.4	3.4	2.51	0.06	5.54	0.09	0.774	0.030
Al24b18	20	49.3	6.1	0.792	0.071	14.8		5.09	0.53	0.120	0.012	6.29	1.68	11.2	2.5	2.09	0.06	4.71	0.11	0.531	0.028
S19(2)b-201: MI reheated (LA-ICPMS)																					
Grain 1																					
Al24c03	50	44.5	3.4	0.925	0.064	14.8		7.34	0.46	0.132	0.008	5.71	0.86	14.6	1.5	2.08	0.04	4.65	0.06	0.256	0.007
Al24c04	25	48.1	3.5	0.998	0.061	14.8		8.61	0.39	0.125	0.008	5.46	0.91	9.9	1.5	1.87	0.04	4.87	0.08	0.223	0.010
Al24c05	40	49.4	5.4	0.647	0.092	14.8		4.23	0.60	0.102	0.012	5.58	1.37	10.9	2.4	2.85	0.07	6.21	0.11	0.362	0.015
Al24c09	15	43.7	7.8	1.329	0.141	14.8		10.43	0.82	0.147	0.017	5.11	2.14	14.8	3.6	1.47	0.06	3.07	0.07	0.182	0.023
Al24c10	60	44.9	2.8	1.086	0.054	14.8		7.76	0.38	0.156	0.007	5.85	0.68	13.8	1.3	1.84	0.04	4.66	0.07	0.200	0.005
Al24c11	35	48.6	3.4	0.913	0.050	14.8		8.27	0.37	0.164	0.008	4.33	0.84	9.7	1.3	2.52	0.05	5.43	0.10	0.295	0.011
Al24c12	18	44.1	6.8	1.428	0.131	14.8		8.73	0.90	0.134	0.017	4.85	1.65	16.0	3.0	1.46	0.06	3.40	0.08	0.113	0.017

na–Not analyzed.

[a] Average EMP value, set to 14.8 wt.% as IS for the quantification of LA-ICPMS signals.

[b] Volatiles are the sum of $H_2O+F+SO_2+Cl$, set to 5.0 wt.% for quantification of LA-ICPMS signals.

Appendix B (*continued*)

	Volatiles	Li		Be		B		Sc		V		Cr		Co		Ni		Zn	
	(wt.%)[b]	(μg/g)	2SD	(μg/g)	2SD	(μg/g)	2SD	(μg/g)	2SD	(μg/g)	2SD	(μg/g)	2SD	(μg/g)	2SD	(μg/g)	2SD	(μg/g)	2SD
S19(2)d-2: MI crystallized (LA-ICPMS)																			
Grain 1																			
Al24a04	5	na		na		na		na		na		na		na		na		na	
Al24a05	5	na		na		na		na		na		na		na		na		na	
Al24a08	5	na		na		na		na		na		na		na		na		na	
Al24a09	5	na		na		na		na		na		na		na		na		na	
Al24a10	5	na		na		na		na		na		na		na		na		na	
Al24b04	5	18	10	21	13	29	18	<17		294	58	641	186	50	17	<130		128	32
Al24b05	5	22	6	17	12	56	17	21	12	458	44	332	92	37	9	<91		92	18
Al24b07	5	27	11	<28		33	17	32	23	360	64	303	223	34	20	204	191	107	37
Al24b08	5	29	8	12	10	37	17	<15		375	43	260	116	32	11	<120		75	22
Grain 2																			
Al24a11	5	na		na		na		na		na		na		na		na		na	
Al24a12	5	na		na		na		na		na		na		na		na		na	
Al24a13	5	na		na		na		na		na		na		na		na		na	
Al24a14	5	na		na		na		na		na		na		na		na		na	
Al24a16	5	na		na		na		na		na		na		na		na		na	
Al24a17	5	na		na		na		na		na		na		na		na		na	
Al24b10	5	13	2	5.5	3.2	25	5	38	6	266	14	<12		36	5	<12		77	7
Al24b11	5	12	3	5.3	7.5	30	9	43	11	284	24	<19		40	8	25	24	77	11
Al24b12	5	10	3	7.4	5.0	26	8	32	8	293	18	<17		40	6	<19		82	9
Al24b13	5	16	5	5.0	8.1	24	10	<50		232	32	<32		31	26	<43		78	17
Grain 4																			
Al24b15	5	30	3	3.7	3.9	28	6	49	8	296	14	165	67	34	4	<24		82	7
Grain 5																			
Al24b16	5	19	8	<78		25	14	<19		303	31	<223		31	13	<153		62	21
Al24b18	5	15	7	13	13	20	12	40	16	245	27	<139		21	11	<147		51	19
S19(2)b-201: MI reheated (LA-ICPMS)																			
Grain 1																			
Al24c03	5	14	2	5.2	4.1	32	5	8.0	7.9	231	19	82	25	65	5	45	31	66	8
Al24c04	5	13	3	8.7	0.9	29	9	<10		269	18	<76		40	5	74	49	64	9
Al24c05	5	18	5	14	3	41	4	80	18	186	31	626	58	16	8	145	68	59	15
Al24c09	5	14	3	<14		20	5	<34		317	44	295		<40		<180		80	26
Al24c10	5	12	1	6.8	0.4	26	4	12	6	366	17	<27		39	3	407	38	75	5
Al24c11	5	24	4	8.0	2.0	40	6	<10		287	18	<80		36	5	<52		86	10
Al24c12	5	11	8	<62		21	5	<23		322	42	<200		42	14	<134		54	25

(continued on next page)

Appendix B (*continued*)

	Rb		Sr		Y		Zr		Nb		Ba		Cs		La		Ce		Nd	
	(μg/g)	2SD	(μg/g)	2SD	(μg/g)	2SD	(μg/g)	2SD	(μg/g)	2SD	(μg/g)	2SD	(μg/g)	2SD	(μg/g)	2SD	(μg/g)	2SD	(μg/g)	2SD
Grain 1																				
Al24a04	88	8	1166	45	37	6	270	23	34	5	na		2.5	1.1	na		138	11	na	
Al24a05	66	5	1020	41	35	8	244	29	30	4	na		1.5	0.6	na		131	12	na	
Al24a08	81	8	1206	50	41	8	277	31	36	5	na		3.7	1.4	na		155	14	na	
Al24a09	90	6	1220	40	36	6	274	21	31	4	na		3.3	0.9	na		147	10	na	
Al24a10	97	7	1114	37	35	7	304	25	33	4	na		3.8	1.0	na		136	11	na	
Al24b04	115	5	1448	52	20	8	229	31	43	3	2398	63	5.4	0.8	95	7	164	13	64	20
Al24b05	103	5	1302	57	38	5	295	22	39	3	2016	69	3.7	0.5	83	5	182	11	88	12
Al24b07	104	5	1139	54	29	9	220	30	35	3	1842	53	3.7	0.7	73	7	137	13	58	21
Al24b08	106	5	1569	58	36	5	260	22	47	3	2487	80	4.1	0.7	96	6	186	11	75	13
Grain 2																				
Al24a11	222	10	745	34	22	7	227	21	21	3	na		13.4	2.0	na		123	10	na	
Al24a12	239	5	933	21	29	3	234	9	28	2	na		16.0	1.0	na		143	5	na	
Al24a13	180	11	815	32	24	5	222	18	18	4	na		11.8	2.1	na		124	9	na	
Al24a14	228	9	797	19	20	3	147	10	28	3	na		15.2	1.7	na		112	6	na	
Al24a16	227	7	815	21	23	7	180	9	22	2	na		13.5	1.1	na		112	5	na	
Al24a17	201	12	804	36	32	7	207	21	22	4	na		13.1	2.2	na		107	10	na	
Al24b10	214	4	891	16	27	1	206	5	22	1	1710	29	14.1	0.5	60	2	131	3	64	3
Al24b11	217	6	886	23	28	2	219	8	21	1	1799	41	14.6	0.8	62	2	131	4	68	5
Al24b12	203	5	894	21	30	2	229	7	23	1	1780	40	12.8	0.7	66	2	138	4	71	5
Al24b13	213	5	867	23	31	3	215	9	21	1	1719	36	13.9	0.8	62	3	128	5	67	7
Grain 4																				
Al24b15	268	6	842	21	36	2	275	7	29	1	1413	30	12.3	0.6	74	2	146	4	74	4
Grain 5																				
Al24b16	258	8	815	29	21	4	165	11	28	2	1443	43	16.1	1.4	61	4	104	6	48	10
Al24b18	214	9	860	30	23	4	170	11	26	3	1259	47	12.0	1.3	55	4	108	6	46	9
Grain 1																				
Al24c03	197	3	935	19	27	2	192	9	25	1	1519	24	11.8	0.9	57	2	108	3	46	4
Al24c04	197	5	708	18	18	2	194	9	23	1	1233	28	10.6	0.9	42	2	74	4	38	5
Al24c05	259	6	1159	31	34	4	188	14	34	2	2108	46	14.4	0.8	82	4	150	6	65	9
Al24c09	116	7	677	31	30	6	241	21	17	3	920	44	7.0	1.2	40	5	77	9	31	15
Al24c10	210	3	949	20	25	1	213	7	25	1	1458	23	11.6	0.3	58	2	119	3	54	3
Al24c11	230	6	1086	25	22	2	191	8	27	1	1816	40	13.3	0.7	63	3	129	4	45	5
Al24c12	136	7	757	34	23	5	250	21	18	2	941	42	7.6	2.9	41	5	91	8	48	13

Appendix B (*continued*)

	Sm		Eu		Gd		Yb		Lu		Hf		Ta		Pb		Th		U	
	(μg/g)	2SD	(μg/g)	2SD	(μg/g)	2SD	(μg/g)	2SD	(μg/g)	2SD	(μg/g)	2SD	(μg/g)	2SD	(μg/g)	2SD	(μg/g)	2SD	(μg/g)	2SD
Grain 1																				
Al24a04	13	8	na		na		4.2	3.7	na		na		na		na		16	2.7	4.5	1.4
Al24a05	31	12	na		na		<4.2		na		na		na		na		11	1.8	4.2	1.0
Al24a08	28	13	na		na		<4.8		na		na		na		na		15	2.8	2.0	1.0
Al24a09	19	8	na		na		3.5	3.1	na		na		na		na		15	1.9	4.9	1.1
Al24a10	13	9	na		na		<3.9		na		na		na		na		14	2.1	5.8	1.3
Al24b04	<18		<2.4		9.2	9.8	<3.3		<0.5		<8.1		1.7	0.6	38.0	3.3	21	1.8	6.9	1.1
Al24b05	14	5	3.8	1.6	11.9	5.3	3.3	2.2	<0.3		6.6	2.8	1.6	0.4	28.8	2.3	16	1.3	5.5	0.7
Al24b07	20	10	<2.9		<9.5		<3.8		<0.6		9.3	5.0	1.1	0.6	31.9	3.4	15	1.7	4.5	0.8
Al24b08	16	7	2.4	1.9	12.9	5.8	2.7	2.5	0.5	0.4	5.2	3.3	1.8	0.5	32.8	2.9	22	1.8	6.7	0.9
Grain 2																				
Al24a11	21	10	na		na		<4.5		na		na		na		na		13	2.0	3.9	1.1
Al24a12	12	4	na		na		1.4	1.6	na		na		na		na		22	1.2	7.1	0.7
Al24a13	17	9	na		na		4.4	3.2	na		na		na		na		17	2.6	5.7	1.5
Al24a14	9	4	na		na		<5.1		na		na		na		na		15	1.7	7.0	1.2
Al24a16	12	4	na		na		<1.6		na		na		na		na		16	1.2	5.5	0.7
Al24a17	10	10	na		na		<3.0		na		na		na		na		18	2.9	3.9	1.3
Al24b10	13	2	3.5	0.4	10.3	1.5	2.0	0.6	0.3	0.1	5.3	0.8	1.0	0.1	32.1	1.1	18	0.6	5.6	0.3
Al24b11	15	3	3.3	0.8	10.0	2.5	1.8	1.0	0.4	0.2	6.1	1.3	1.0	0.2	27.9	1.6	18	0.9	5.7	0.5
Al24b12	14	2	3.7	0.6	12.0	2.2	2.7	0.9	0.4	0.1	5.5	1.1	1.0	0.2	29.4	1.5	18	0.9	5.8	0.5
Al24b13	15	4	3.8	1.1	13.0	3.3	<1.8		0.3	0.2	5.5	1.7	0.8	0.2	31.7	1.9	18	1.0	5.4	0.5
Grain 4																				
Al24b15	17	2	3.9	0.6	12.2	1.8	3.0	0.8	0.4	0.1	8.0	0.9	1.1	0.2	18.7	0.9	19	0.7	6.3	0.4
Grain 5																				
Al24b16	11	6	<2.5		7.3	5.3	2.6	1.9	0.3	0.3	4.5	2.3	0.9	0.3	40.3	3.1	20	1.6	6.5	0.9
Al24b18	11	5	2.6	1.5	8.6	4.5	<2.8		0.3	0.3	2.5	2.0	0.9	0.4	31.0	3.1	24	2.0	7.7	1.1
Grain 1																				
Al24c03	12	2	2.8	0.6	8.5	2.1	2.2	0.9	0.4	0.1	5.5	1.2	1.1	0.1	24.8	0.9	17	0.6	5.6	0.3
Al24c04	8	3	2.4	0.8	6.6	2.6	1.7	1.1	0.2	0.1	5.2	1.4	1.0	0.2	29.1	1.5	15	0.8	4.4	0.4
Al24c05	16	5	4.5	1.2	10.1	4.1	3.2	1.8	0.3	0.3	<12.5		1.4	0.3	31.4	1.9	25	1.2	7.9	0.6
Al24c09	13	8	3.2	2.5	<8.4		4.2	3.5	<0.5		10.1	4.4	0.4	0.4	16.3	2.9	10	1.6	3.2	0.8
Al24c10	11	1	2.8	0.4	7.5	1.3	2.1	0.5	0.4	0.1	5.5	0.8	1.2	0.1	24.3	0.7	18	0.5	5.9	0.2
Al24c11	10	3	2.2	0.8	7.3	2.4	1.6	1.0	0.3	0.2	6.5	1.4	1.4	0.2	29.7	1.5	20	1.0	6.8	0.5
Al24c12	9	7	3.5	2.1	7.0	6.7	<2.8		<0.4		8.4	3.5	0.8	0.4	13.4	2.7	13	1.6	4.1	0.9